Separation and Purification Technology 415 (2026) 139723

Contents lists available at ScienceDirect

Separation and Purification Technology

journal homepage: www.elsevier.com/locate/seppur

Influence of pleat geometry on the operating behavior of cleanable surface filters in a test-rig with pulse-jet-cleaning

Jakob Paul Knisley *, Julian Martin Schlegel, Jörg Meyer, Achim Dittler

Karlsruhe Institute of Technology, Institute of Mechanical Process Engineering and Mechanics, Straße am Forum 8, Karlsruhe, 76131, Germany

ARTICLE INFO

Communicated by Volodymyr Tarabara

Keywords:
Surface filtration
Pleated filter medium
Filter medium characterization
Lab testing

ABSTRACT

The influence of pleat geometry on the operating behavior of cleanable surface filters was investigated using harmonized regeneration conditions and complementary modeling approaches. An adapted DIN ISO 11057 procedure was applied to isolate geometric effects for differently aged filter media by maintaining consistent regeneration intensity, raw gas concentration, and filter media face velocity across all geometries. The results demonstrate that under these harmonized experimental conditions pleat geometry influences the operating behavior from the first filtration cycle. The resulting differences in cycle time, residual differential pressure, and clean gas particle number concentration persist for the duration of the experiments. While aging leads to increased residual differential pressure and reduced particle emissions, similar trends across all geometries indicate comparable macroscopic aging behavior. No significant loss of effective filter media surface area was observed for the different geometries under the investigated operating conditions using a coarse, free-flowing test dust. A geometric model describing dust deposition on pleat sidewalls and in the pleat bottom suggests that the observed differential pressure development can be explained by the dust deposition inside the pleat in combination with the pleat geometry. In summary, the results show that increasing the pleat ratio leads to a shorter cycle time under the investigated harmonized conditions, and the geometry influence was evident from the very first cycle.

1. Introduction

Surface filters are widely applied in different industries to comply with emission limits or for product recovery. Compared with depth filters, the particles are mainly collected on the surface of the filter media. The resulting particle layer, the so-called dust cake, is a highly efficient separator for particles from particle-laden gas streams [1]. Generally, surface filters are operated cyclically, with each cycle consisting of a filtration and a regeneration phase. During the filtration phase, dust accumulates on the surface of the filter medium, resulting in a progressively thickening dust cake. This leads to an increase in differential pressure between raw and clean gas side, due to the increasing flow resistance of the dust cake. To reduce the differential pressure, the filter medium is regenerated periodically. The regeneration (partially) removes the dust cake, resulting in a residual differential pressure, which is lower than before the regeneration of the filter media, but does not return to the differential pressure of a clean, unused filter medium [2]. A widely used method for regenerating cleanable filter media is the use of a short pulse of pressurized air directed against the nominal flow of the gas through the filter media (pulse-jet). During regeneration, the pulse intensity must be sufficiently strong to counter the main flow direction and reverse the flow through the filter media [3]. Flow reversal can result in the detachment of the dust cake due to the flow force of the reversed flow through the filter cake, the inertia of the dust cake, and the acceleration and deceleration of the filter media, as well as shear forces inside the dust cake and between the dust cake and the filter media [2]. The completeness of dust cake removal directly affects the operating behavior of surface filters. An insufficient removal of dust (patchy cleaning) can result in a transient differential pressure increase due to the non-uniform flow through the filter media and/or permanent blocking of a part of the filter media [4]. Furthermore, regeneration frequency and the particle emission are linked to the efficiency of dust removal, as a higher residual pressure results in a shorter filtration cycle (for a set maximum differential pressure) and therefore requires more frequent filter medium regeneration and leads to an increase in particle emission, as the highly efficient dust cake is removed [1,5]. More frequent regeneration also increases the mechanical stress experienced by the filter media due to the pulse-jet [2].

Different designs of surface filters exist, with a common design being the use of pleated (folded) filter media in a panel or cartridge design [1,6]. The filter medium is pleated to increase the available

* Corresponding author.
E-mail address: jakob.knisley@kit.edu (J.P. Knisley).

https://doi.org/10.1016/j.seppur.2026.139723
Received 23 May 2026; Received in revised form 29 July 2026; Accepted 11 August 2026
Available online 18 August 2026

filter media surface area, either to accommodate spatial boundaries for the filter system or to reduce the differential pressure of an existing filter system by increasing the surface area in the existing filter system. The seemingly advantageous increase in filter media surface area is accompanied by the disadvantage that pleating the filter media and operating pleated filter media elements can influence the operating behavior of surface filters. Even in the absence of dust, pleated filter elements can exhibit certain problems, when fluid flows through them. Due to deformation of the filter medium during fluid flow, the effective filter media surface area can be reduced when neighboring pleats close up. Pleat closure is a result of a high pleat density, where pleats can interact with each other, either by being forced apart by fluid or being dragged together by viscous forces of the fluid [7,8]. The closure leads to an increase in differential pressure due to the loss of effective filtration area. The filter medium can also be compressed (especially in the pleat bottom and the pleat tips) as a direct result of the pleating process or hydrodynamic effects. Compression alters the permeability of the filter medium and affects the development of differential pressure, as the combined compression and effective area loss results in a higher differential pressure even for dust free filter systems [8,9].

Numerous experimental and numerical studies have been conducted in the past concerning pleated filter elements and media for depth and surface filtration with regard to dust deposition inside the pleats, the development of differential pressure and, for surface filters, the dust cake removal. The following paragraphs provide an overview of existing research for both depth and surface filtration, but focus on relevant phenomena for surface filters.

A key aspect of evaluating pleated filter media is the geometry of the pleats, often quantified by the pleat ratio (PR). The PR describes the ratio of pleat height to pleat width, with a high pleat ratio resulting in more pleats per filter element length compared to a low PR. Increasing the pleat ratio influences the development of differential pressure and the dust loading of the pleats. Numerical studies in particular have focused on this relationship for model pleats and pleated filter cartridges. Increasing the pleat ratio leads to an increasing inlet velocity into the pleat and a non-uniform velocity distribution over the length of the pleat. The increased inlet velocity results in more viscous drag and leads to higher differential pressure even in the absence of dust [10–13]. The inhomogeneous flow inside the pleat leads to a change in streamlines, which affects the deposition location of particles inside the pleat and the filter media. The inhomogeneous cake build-up results in an increase of differential pressure [14–16]. A high inlet velocity in combination with a high pleat ratio leads increased particle deposition in the pleat bottom, resulting in a non-homogeneous dust cake [15,17–19]. As dust not only accumulates in the pleat bottom, but also on the sidewalls of the pleat during filtration, the flow distribution inside the pleat can become inhomogeneous. The uneven flow distribution can result in further uneven particle deposition inside the pleat which results in an increase in differential pressure [18,20,21]. Although these studies provide important insight into flow and deposition mechanisms within pleats, many are based on numerical simulations or simplified geometries and do not consider repeated filtration and regeneration cycles typically carried out for filter elements in surface filtration.

In addition to dust deposition, the dispersity of the particles in combination with the PR influences the cake build-up, where large particles tend to migrate to the bottom of the pleat due to inertia, while fine particles form a more homogeneous dust cake on the sidewall of the pleats. The resulting non-uniform dust cake leads to the blocking of surface area by particles in the bottom of the pleat or by forming dendritic structures, which can block the underlying filter surface area during filtration [21–23]. This blocked surface area again can result in a steeper increase of differential pressure over the course of the service life of the filter element. In summary, a higher pleat ratio results in a steeper increase in differential pressure due to non-uniform flow distribution and dust deposition within the pleat, which further increases the non-uniform flow inside the pleat and through the filter media.

The experimental research on pleated surface filters is mainly focused on two key aspects: the regeneration of pleated filter elements (panel and cartridge) and the eventual loss of effective filtration area during continuous operation. The main cause of effective surface area loss is the accumulation of dust inside the pleats, leading to temporary or permanent blockage of effective filtration area. This phenomenon is often cited as the cause for cycle time reduction and residual pressure increase [24–27]. For both, pleated cartridges [24,25,28] and panels [26,27], an increasing PR is associated with a lower effective filtration area during dust loading, which leads to an increase in differential pressure at constant volumetric flow rate through the filter element. In addition, Teng et al. [29] showed, that after exceeding a PR of 5 the increase of differential pressure increases strongly due to blockage of the pleats by the dust, and thus reducing the effective filter media surface area.

In experimental investigations, the PR is often increased by using different filter elements with different filter media surface areas, while keeping the length and the diameter of the element constant. Certain operating parameters, such as dust feed rate and volumetric flow, are adapted to enable comparison between the filter elements with different surface area. However, the regeneration intensity is often not adapted [25,28,30]. With increasing filter media surface area, the same regeneration parameters (tank pressure and electric valve opening time) lead to a less thorough cleaning of the filter media, as the pulse intensity is reduced due to the larger filter media surface area to be cleaned. This makes it difficult to distinguish purely geometric effects from operational influences on the (irreversible) reduction of the available filter media surface area. Li et al. [31] varied the PR while keeping the surface area constant, and thus the regeneration parameters were not adapted. They found that increasing the pleat ratio for panel filters leads to a higher residual differential pressure and a shorter cycle time over the first nine cycles of new, non-aged filter media when regenerating the filter media by back-blowing. Furthermore, they found that the pleat ratio influences the slope of differential pressure increase [31]. However, the regeneration intensity was not characterized for the investigated pleat geometries, and the study was limited to the first nine filtration cycles of new, non-aged filter media regenerated by back-blowing. Consequently, the influence of pleat geometry under harmonized regeneration conditions for pulse-jet cleaning and after long-term aging remains partially unclear.

A wide range of studies has investigated the regeneration and dust cake removal from pleated filter elements. For effective filter medium regeneration the maximum peak pressure, as a result of flow reversal by the pulse-jet and the uniformity of the peak pressure across the filter element are often considered. Uniformity is essential to avoid patchy cleaning for large filter elements and ensure a near-complete dust cake removal and the maximum peak pressure should exceed 400–500 Pa. These values should be exceeded to sufficiently reverse the flow during regeneration, as pleated filter elements often allow little to no filter media movement, making the reversal of flow the dominant regeneration mechanism [32,33]. Studies have investigated the deflection of the pulse-jet, which leads to varying peak pressures dependent on the distance of the blow pipe and the angle of the blow pipe opening [34]. The installation of cones (pleated and non-pleated) was investigated by Li et al. [35] and Qiu et al. [36] to increase the maximum peak pressure and uniformity of regeneration across the height of the element, showing that using a cylindrical inner cone leads to an increasing uniformity and height of the maximum peak pressure. The effect of an induced airflow on the maximum peak pressure to increase its magnitude and improve uniform pressure distribution in filter cartridges was investigated by Yan et al. [37], showing that an induced airflow assists with uniformity of the peak pressure across the height of a cartridge. Li et al. [38] found that increasing the peak pressure reduces the residual dust on the filter element, correlating a high peak pressure with effective filter element regeneration. Other operating parameters, such as tank pressure, electromagnetic valve opening time [39], and clean-on-time or clean-on-demand modes [6,40] have also been investigated, offering advice for what PR what regeneration mode should be used. Xing et al. [41] investigated different nozzle shapes, showing that using a slit nozzle increases the pressure uniformity of regeneration compared to a typical, circular nozzle. Xie et al. [42] tested the simultaneous pulse-jet regeneration from the top and the bottom of a filter cartridge, with the result that regenerating the cartridge from both sides yields the highest peak pressure and the longest cycle time with the lowest residual differential pressure. The large number of studies highlights the importance of effective regeneration for stable and economical filter operation. However, while regeneration parameters have been investigated extensively, few studies have systematically harmonized the regeneration conditions when comparing different pleat geometries. Consequently, the isolated influence of pleat geometry on filter operation under comparable regeneration intensities has not yet been fully clarified.

Furthermore, the size of the separated particles is relevant for filter element operation and regeneration. Small particles can irreversibly block filter media pleats due to stronger adhesive and cohesive forces between the particles and the filter medium [43–45]. Irreversible clogging leads to non-uniform dust deposition and velocity distribution within the pleats because, after regeneration, the non-blocked surface area offers lower flow resistance and the dust-laden gas preferentially flows through these patches. This leads to local increases of the face velocity and different cake heights across the surface of the filter media and results in shorter filtration cycles due to a steeper differential pressure increase [44,45].

Despite the existence of numerous studies investigating pleated filter elements under various criteria, the isolated influence of pleat geometry on filter operation remains insufficiently understood, as many studies simultaneously vary filter surface area and regeneration conditions. This makes it difficult to distinguish geometric effects on operating behavior, particularly with respect to irreversible surface area loss, residual pressure development, and cycle time development.

Therefore, the objective of this study is to systematically investigate the effect of filter medium geometry on the operating behavior of surface filters under harmonized operating and regeneration conditions. To achieve this, a methodology employing harmonized experimental parameters (maximum peak pressure, raw gas concentration, and filter medium face velocity) and identical filter media, based on the DIN ISO 11057 standard [46] is applied [47]. This allows the isolated evaluation of the effects of filter medium geometry and medium age on filter operation. Furthermore, the comparison of flat and pleated geometries under standardized conditions and a consistent experimental procedure enables an assessment of the transferability of flat media coupon tests to pleated filter media.

To evaluate the geometry influence, the different filter media geometries were investigated in a test-rig with pulse-jet cleaning in accordance with DIN ISO 11057. Differences in cycle time, residual differential pressure, and particle emission can thus be directly correlated to the respective geometry of the filter media.

In addition, a simple model describing the time-dependent dust loading of filter media pleats and the permanent blockage of filter media surface area by dust is introduced to qualitatively describe differential pressure increase as a result of the influence of filter medium geometry.

2. Methodology

2.1. Experimental setup, methodology and materials

2.1.1. Filter media test-rig

The test-rig for conducting experiments is based on the international guideline DIN ISO 11057 and is depicted schematically in Fig. 1.

The dust is dosed and dispersed by a rotating brush dust feeder (NDF 100 BD, Filtration Testing Equipment & Services GmbH). The generated aerosol is neutralized using a KR-85 neutralizer. The neutralized aerosol is drawn through the raw gas duct, and the raw gas concentration is continuously monitored by extinction measurement. The dust-laden air is partially drawn through the filter medium, while the cleaned gas is released into the ambient air as excess air after passing through an absolute filter (Versapor, Pall Corporation). The remaining dust-laden gas stream is drawn through the raw gas duct, cleaned using a filter cartridge (Viledon®, Freudenberg Filtration Technologies GmbH & Co.KG), and then released into the ambient air. Mass flow controllers are used to regulate the volumetric flow rates through the raw (5853S, Brooks® Instruments) and clean gas duct (SLA 5851, Brooks® Instruments). The raw and clean gas flow are indicated in Fig. 1 as the dark and light blue arrows, respectively.

After either surpassing a set differential pressure or a defined time interval, the filter medium is regenerated by pressurized air (pulse-jet) to dislodge the dust cake and reduce the differential pressure between the raw and clean gas side. When regeneration is triggered, an electromagnetic valve (262, ASCO™) opens and releases pressurized air through the blow pipe (3.3 cm diameter) and the nozzle (0.3 cm diameter) directed towards the filter medium. The pressurized air is supplied by the in-house pressurized air system, and the pressure inside the pressure tank (Hosokawa Mikropul) with a tank volume of 2.3 L is controlled by a pressure regulator (ITV3050, SMC) to set the desired regeneration pressure.

Unlike DIN ISO 11057, the particle emission is not measured gravimetrically, but with an optical particle counter (OPC). The measurement principle of the Promo® 2000 with a Welas® 2300 sensor by the manufacturer Palas® is based on optical light scattering of white light by single particles. The sensor was calibrated using MonoDust 1500 provided by Palas® with an equivalent scattered light diameter of 1.26 μm. The Welas® 2300 has a detection limit of $4 \cdot 10^4$ particles cm^{-3}. The sampling point on the clean gas side was positioned 80 cm behind the backside of the filter media. The particle counter enables time- and size-resolved measurements of the particle number concentration, providing a more detailed evaluation of emission events compared to gravimetric measurement. The measurement range of the sensor was set to the smallest range of 0.2–10 μm to better capture the size range of the most penetrating particle size (MPPS) of surface filters, which is assumed to be between 0.3–1 μm [5]. Below 0.2 μm the counting efficiency of the optical is reduced, because air molecules start to scatter the light, resulting in false counting events from the OPC. The emission measurement was primarily used for monitoring the clean gas emissions.

2.1.2. Filter medium

The filter medium used to characterize both the flat and pleated geometries in the test-rig consisted of thermally bonded PES fibers with an ePTFE membrane on the upstream side. The medium has a thickness of 0.09 cm. The membrane is laminated onto the fibers to enhance dust separation efficiency and reduce dust penetration into the filter medium. Furthermore, the membrane can facilitate the dislodging of the dust cake during regeneration. This filter medium has a base weight of $290\,g \cdot m^{-2}$ and an air permeability (at 200 Pa) of $35\,L \cdot dm^{-2} \cdot min^{-1}$. Both geometries, flat and pleated, were fabricated from the same filter medium, allowing a comparison of their operating behavior, without the influence of differences in material properties. Nevertheless, slight sample-to-sample variations in filter media resistance and the homogeneity of the laminated ePTFE membrane cannot fully be excluded.

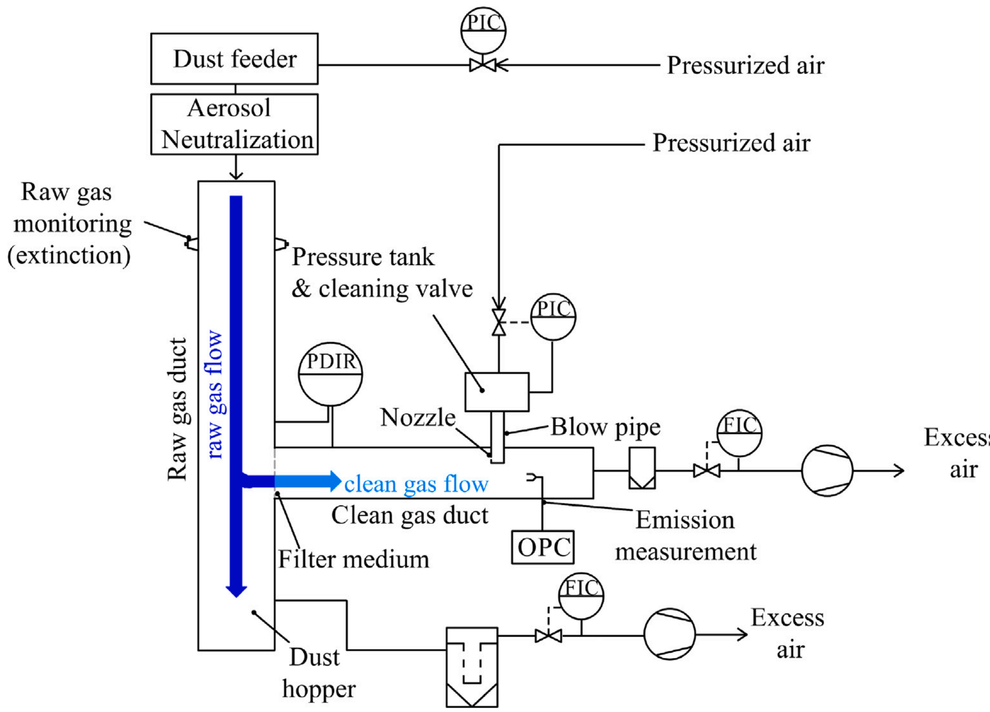

Fig. 1. Schematic of the adapted filter media test-rig with pulse-jet-cleaning based on DIN ISO 11057.

2.1.3. Configuration of different pleat ratios for testing

Due to differing filter media geometries, both flat and with varying pleat ratios, the filter media samples are implemented differently into the test-rig. The flat filter medium coupon is implemented into the test-rig as intended by the DIN ISO 11057 standard. A circular metal filter holder with a flow cross-section of $154\,\mathrm{cm}^2$ is used. The filter medium is placed into the holder, and a support bar structure for more stability is added on the clean gas side behind the filter medium. If correctly dimensioned the filter holder with the flat filter medium is self-sealing. The flow cross-section corresponds to the implemented filter media surface area of $A_{\mathrm{Filter}} = 154\,\mathrm{cm}^2$ for the flat geometry. PR0 was included as a flat reference geometry. Although its filter media surface area and holder geometry differ from those of the pleated samples, the operating conditions at the filter media face were harmonized to enable comparison of the operating behavior.

The pleated filter media geometries are implemented differently. To stabilize the pleated structure and ensure sealing, a two-part 3D-printed structure is used to fix the filter medium inside the holder with a set PR. The filter medium is sealed within the structure using silicone. The two-part structure is then inserted into a circular metal filter holder and the gap between the structure and the metal filter holder is sealed using a gasket.

As this study aims to compare different pleat ratios under identical experimental conditions, the implemented filter medium surface area for the pleated geometries was kept constant at $A_{\mathrm{Filter}} = 320\,\mathrm{cm}^2$ for all pleat ratios, corresponding to nine pleats for each filter element. The pleat ratio (2–5) is adjusted by varying the distance between pleats (P_{Width}) while maintaining constant pleat height (P_{Height}). A pleat ratio of 1 is omitted due to the assumed negligible influence of very shallow pleats. The distance between the pleats is changed by reducing the cross-flow section of the 3D-printed structure, forcing the pleats closer together. Pictures (front view) of the different filter holders and a schematic showing the cross-sectional view and the reduction of the distance between the pleat tips, thus increasing the PR, are depicted in Fig. 2. The difference in filter surface area between the flat and the pleated geometry was due to the effort to implement as much pleated filter media surface area as possible within the existing circular boundaries of the clean gas duct.

Table 1
Summary of geometric data for the different pleating variants of the filter media.

Geometry	P_{Height}/cm	P_{Width}/cm	Actual PR	$A_{\mathrm{Cross\text{-}section}}$/cm^2	A_{Filter}/cm^2
PR0	–	–	–	154	154
PR2	1.96	1.0	1.96	81	320
PR3		0.67	2.93	54	
PR4		0.5	3.92	40.5	
PR5		0.4	4.90	32.4	

As shown in Fig. 2 the reduction of the cross-flow section for the pleated filter medium leads to an increase of the PR. The number of pleats and the implemented filter media surface area remained unchanged. The reduced cross-flow section forces the pleats closer together, resulting in a higher PR. The flat filter medium is depicted for the sake of completeness, even though no pleating occurred. The designations PR2–PR5 are nominal labels based on the actual PR and are obtained by rounding for simplicity. The geometric dimensions and the corresponding actual PR for each pleated variant are summarized in Table 1. As a result of changing the pleat width, the pleat height changes slightly, but owing to the small pleat opening angles, the vertical pleat height is approximately equal to the pleat sidewall length, which remains unchanged. Further details are given in Appendix A.

2.1.4. Harmonization of experimental parameters

Due to differences in filter media surface area (flat vs. pleated) certain experimental parameters must be adapted to ensure comparability. The clean gas flow $\dot{V}$ is increased for the pleated geometries to maintain the same filter medium face velocity w_{Filter} and the dust dosage rate is adjusted to achieve the same raw gas concentration $c_{\mathrm{Raw\ gas}}$. A comparative overview of the experimental parameters is listed in Table 2.

For meaningful comparison, the different filter media geometries should be regenerated with the same intensity. In this study, the maximum differential pressure caused by the pulse-jet at the same electrical valve opening time t_{Valve} was used as a reference and target variable for the intensity. This is consistent with previous studies, which

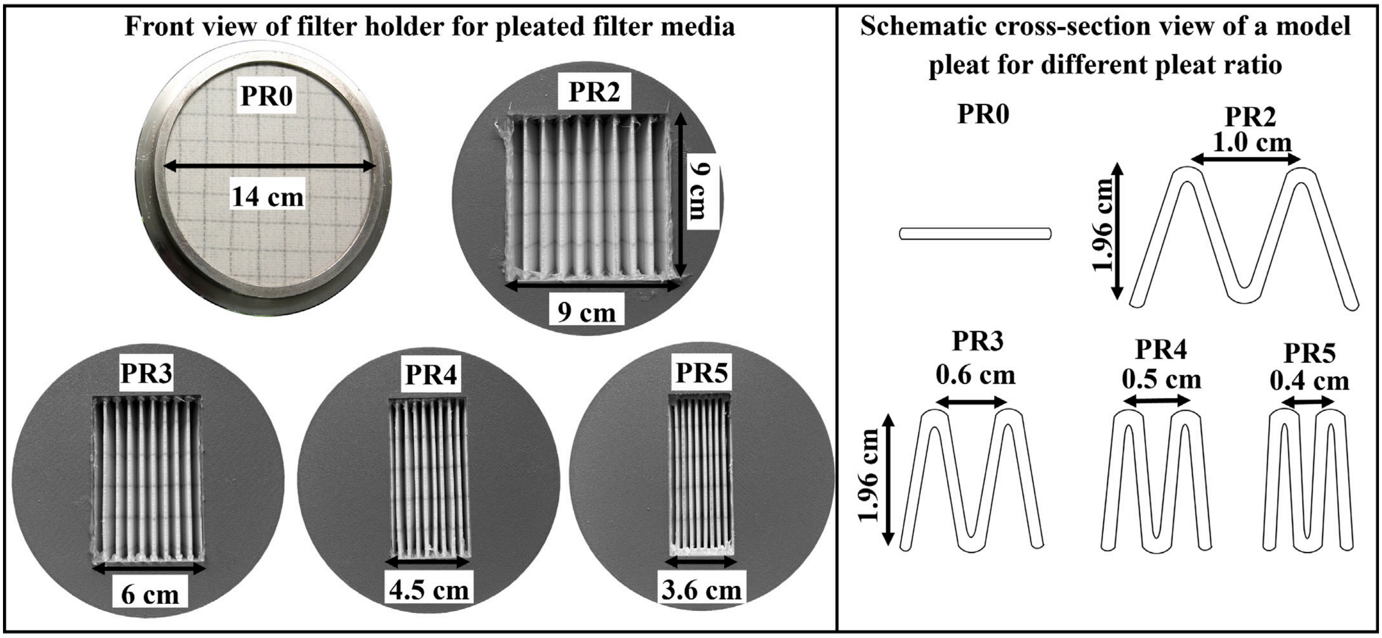

Fig. 2. Front views of the filter holders for the flat and pleated filter media (left) and schematic cross-sectional views illustrating the reduction in pleat spacing with increasing pleat ratio (right).

consider the maximum peak pressure as a governing parameter for regeneration intensity evaluation [33,35,37,38]. Besides the maximum peak pressure, the duration of the differential pressure pulse was also evaluated. Since the electric valve opening time was kept constant for all geometries, the pulse duration was similar for all geometries (700–750 ms). The corresponding pressure–time curves and additional information on the harmonization of the regeneration intensity are provided in Appendix B. The intensity measurements were conducted using a fast differential pressure sensor (DS-010, Kalinsiky Sensor Elektronik GmbH & Co. KG). The maximum peak pressure during regeneration was measured directly on the surface of the flat filter medium and inside the pleats for the pleated geometries on the raw and clean gas side. The specific experimental setup and detailed explanation of the measurement and the adaptation of the tank pressure for regeneration of a flat and a pleated geometry are shown in our previous study [47].

The results of the intensity measurements for PR0 are shown in Fig. 3 on the left. The intensity for each tank pressure p_{Tank} was measured ten times and the depicted data points represent the mean value of the ten measurements. The error bars represent standard deviation. Due to the linear dependency of the maximum peak pressure to the tank pressure, the required tank pressure for the flat filter medium for certain maximum peak pressures can be calculated. The intensities measured for the pleated filter media geometries (at a tank pressure of 0.5 MPa) and for the adapted tank pressure for the flat filter medium are depicted in Fig. 3 on the right. Again, each data point represents the mean value of ten intensity measurements and the error bars quantify standard deviation. The maximum peak pressure for the flat filter medium at a tank pressure of 0.5 MPa is 2.2 times higher than the intensity of the pleated geometries at $p_{\text{Tank}} = 0.5\,\text{MPa}$. This is due to the increase of filter medium surface area for the pleated geometries. The increase in surface area results in a decrease in regeneration intensity, because the volumetric flow from the regeneration system counteracting the nominal flow of the gas remains unchanged for the same regeneration settings ($p_{\text{Tank}}, t_{\text{Valve}}$). This results in a decrease in regeneration force per unit filter media surface area for the pleated samples. Thus, to keep regeneration conditions constant, the tank pressure for PR0 has to be reduced.

Tank pressure for the flat filter medium is lowered to 0.19 MPa (calculated value from the linear regression). Further measurements for the flat filter medium with the reduced tank pressure were conducted, which resulted in the data point in the right graph in Fig. 3 (indicated by the arrow). The reduction of the tank pressure for the flat medium and the measurements for the differently pleated geometries show a similar maximum peak pressure with a negligible relative deviation of 5% around the mean value of 1134 Pa (indicated by the dotted line). This enables the comparable regeneration for the different geometries with respect to the maximum peak pressure.

2.1.5. Experimental methodology and parameters

To characterize and compare the different filter media geometries, the experimental procedure outlined in the DIN ISO 11057 guideline was adapted. A schematic depicting the experimental procedure is shown in Fig. 4.

The experimental procedure for characterization of cleanable filter media consisted of three phases, where each phase should represent a different stage in the life cycle of the filter medium. A detailed description of the adapted procedure from DIN ISO 11057 is provided by Knisley et al [47]. The first phase started with a new filter medium sample and consisted of three Δp-controlled cycles with regeneration using a pulse-jet after exceeding a given differential pressure threshold Δp_{Max} between raw and clean gas side of 500 Pa. These cycles were conducted to assess the behavior of a factory-new filter medium, such as initial particle penetration of the new, non-aged filter media or the development of the differential pressure during the first cycle. The second phase (aging) consisted of an accelerated laboratory aging procedure intended to reproduce the effects of repeated filtration and regeneration on the filter media. The aging stage in this study consisted of 500 Δt-controlled cycles with a cycle duration t_{Cycle} of 30 s, resulting in a regeneration of the filter medium every 30 s. The aim of the aging stage was to stabilize the operating behavior in respect to particle number concentration and development of residual differential pressure. A stable aging state was assumed if the slope of the differential pressure and particle number concentration during the last 100 aging cycles remained below predefined thresholds of 0.1 Pa cycle^{-1} and 4 particles cm^{-3} cycle^{-1}, respectively. Detailed explanations are provided in Section 3.2. Following the accelerated aging phase, 10 stabilizing (required to stabilize experimental parameters after aging) and 30 measurement cycles (both Δp-controlled) with regeneration

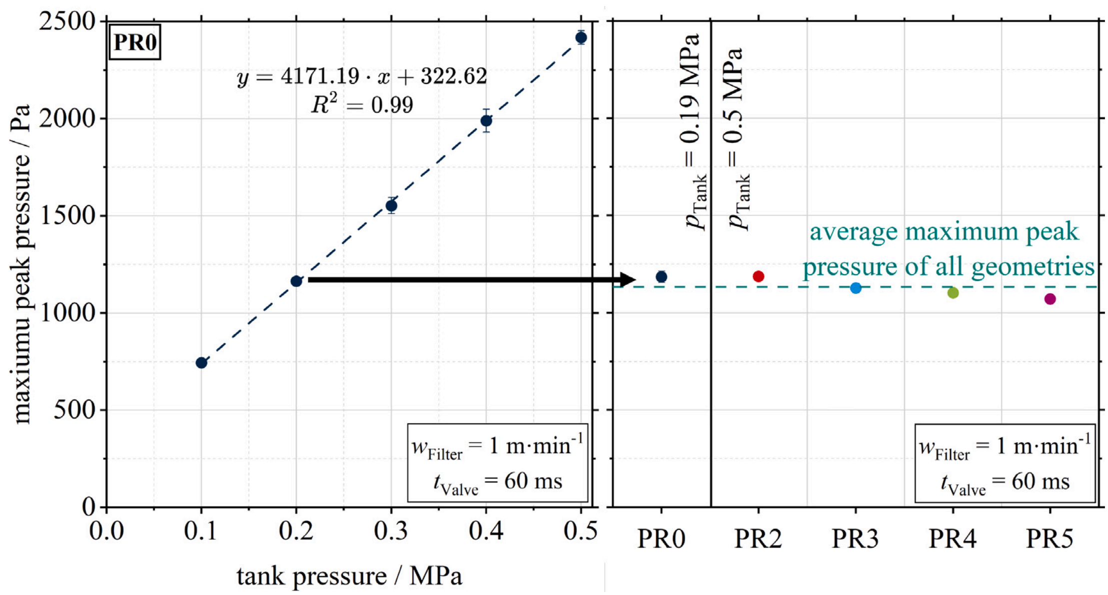

Fig. 3. Mean maximum peak pressure dependent on tank pressure for the flat filter medium geometry (left), and mean maximum peak pressures obtained for PR0 and PR2–PR5 under harmonized regeneration conditions (right). Error bars indicate the standard deviation of ten measurements at $t_{\text{Valve}} = 60\,\text{ms}$.

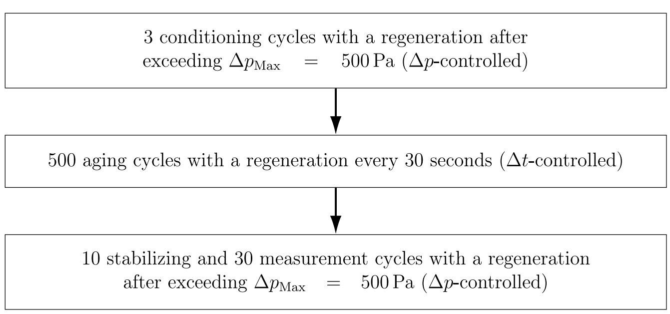

Fig. 4. Adapted experimental procedure consisting of conditioning, accelerated aging, stabilization, and measurement cycles.

Table 2
Experimental parameter for the flat and pleated filter media geometries.

	A_{Filter}/ cm^2	w_{Filter}/ m · min^{-1}	c_{Raw}/ g · m^{-3}	Δp_{Max}/ Pa	p_{Tank}/ MPa	t_{Valve}/ ms	t_{Cycle}/ s
PR0	154	1	10	500	0.19	60	30
PR2–PR5	310	1	10	500	0.5	60	30

at a differential pressure of 500 Pa were conducted. These cycles are essential to characterize and evaluate the operating behavior of the different filter media geometries. The procedure was performed for the flat and pleated geometries of the same filter media. To evaluate the operating behavior, the development of differential and residual differential pressure, the cycle time between regenerations, and the particle number concentration in the clean gas were considered.

The experimental parameters influencing the operating behavior of surface filters are characterized in DIN ISO 11057 and were adapted in this study. The experimental parameters for the flat and the pleated geometries are listed comparatively in Table 2. The filter medium surface area varies between the flat and pleated geometries, as explained in Section 2.1.3. This meaning that the tank pressure has to be adapted for the flat filter medium to ensure the same intensity of regeneration, represented by the maximum peak pressure. The detailed explanation of the adaptation of p_{Tank} is given in Section 2.1.4. The filter medium face velocity in this study was adjusted to $w_{\text{Filter}} = 1\,\text{m} \cdot \text{min}^{-1}$, to reproduce typical operating conditions for pleated or pleatable filter media and elements according to VDI 3766 [48]. To enable the same filter medium face velocity, the volumetric flow through the clean gas duct has to be increased for the pleated geometries. As a result of the increased volumetric flow the dust dosage rate also has to be increased to generate the same raw gas concentration for both flat and pleated geometries. The raw gas concentration is measured gravimetrically by flowing through a filter medium sample for a set amount of time (6 min) and weighing the sample before and after the loading process. With a known volumetric flow, the raw gas concentration can then be calculated [46].

2.1.6. Test dust

The test dust used was the coarse Boehmite (AlO(OH)) PURAL®SB by (Sasol) with $x_{50,3} = 25\ \mu\text{m}$. The cumulative mass-based particle size distribution, measured using laser light ensemble scattering (Sympatec Helos & Rodos dry disperser), is shown in Fig. 5.

The dust is non-agglomerating and free-flowing, making it easy to dose and beneficial for regeneration due to an easy removal of the dust cake. Previous studies [49,50] using the same test dust have shown that it leads to reliably detectable emission events on the clean gas side after regeneration, despite its low fine-dust fraction. This indicates that a sufficient number of particles in the assumed size range of the MPPS for surface filters is present and capable of penetrating the filter medium, especially for the free-flowing test dust.

2.2. Model concepts of differential pressure development for pleated filter media

For the evaluation of the differential pressure development for the different filter media geometries, two simple approaches were chosen and are discussed in this study. Previous studies [24–28] often identify the reduction of effective filter media surface area, and the resulting increase of filter media face velocity due to dust deposition inside the pleats as a determining factor for the differential pressure development.

However, reduction of effective filter media surface area can occur in different ways, depending on whether the area loss is temporary or permanent: effective filter media surface area can either be lost permanently over many subsequent cycles or can be periodically blocked within a cycle and released in the regeneration process. Both mechanisms are described and discussed in the following sections.

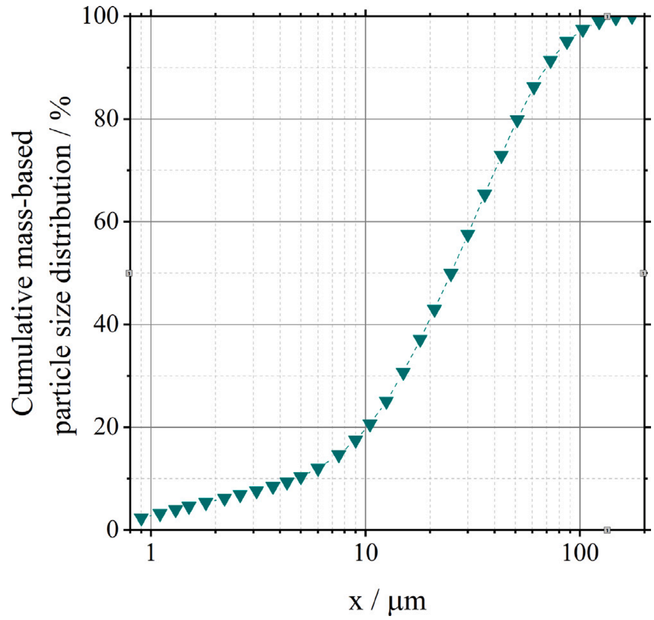

Fig. 5. Cumulative mass-based particle size distribution of PURAL®SB measured with Sympatec Helos & Rodos dry disperser.

2.2.1. Reversible reduction of filter media surface area during a filtration cycle

The simple, geometric model discussed in this section addresses the (reversible) accumulation of dust inside a model pleat, with the aim of reproducing the differential pressure increase for differently pleated filter media (excluding reference geometry PR0) within one filtration cycle. The model idea consists of two different mechanisms of dust accumulation inside the pleat. The two resulting, limiting models are schematically depicted in Fig. 6.

Initially, the model pleat, whose geometric data is listed in Table 3, is dust free, and no dust is assumed to be deposited inside the filter medium during the model calculations. The dust cake is assumed to be incompressible. As a result of dust accumulation, the effective filter media surface area is reduced at the pleat bottom by the deposited dust, leading to an increase in filter medium face velocity under the assumption of constant volumetric flow through the pleat. The difference between the model concepts lies in the mechanisms of dust accumulation.

In Fig. 6 a new, dust-free pleat with the available filter media surface area (indicated in green) is depicted. During filtration (after a certain amount of elapsed time Δt) for the bottom filling model all separated dust accumulates in the pleat bottom, forming a non-permeable dust cake (shown in red). With increasing filtration time the height of the non-permeable dust cake increases, thereby reducing the available filter media surface area. The resulting increase in differential pressure is solely attributed to the increasing filter medium face velocity and the filter medium resistance of the clean filter medium. This model concept may describe conditions with very narrow pleats and coarse test dust, where high inlet velocities cause particles to deposit predominantly in the pleat bottom due to inertia.

The sidewall cake growth is shown in Fig. 6 on the bottom. Here, the dust cake grows homogeneously along the sidewalls of the pleat, while remaining permeable (indicated by the lighter red shading). Only the dust accumulated in the pleat bottom, below the intersection of the growing sidewall cakes, remains non-permeable. This simplification is permissible, because the flow path through the dust cake in the pleat bottom is significantly longer than the flow path through the dust cake on the sidewalls. This results in a reduction of effective filter media surface area over time, as well as a thickening dust cake with increasing resistance due to higher areal dust loading on the sidewalls. Both effects contribute to an increase in differential pressure.

Table 3
Summary of data used for the model calculations of the differential pressure increase within a filtration cycle.

Parameter	PR2	PR3	PR4	PR5
b_0/m	$9.5 \cdot 10^{-3}$	$6.3 \cdot 10^{-3}$	$4.7 \cdot 10^{-3}$	$3.8 \cdot 10^{-3}$
s_0/m		0.019		
L/m		0.09		
ρ/kg · m^{-3}		2800		
ε/−		Variable		
$c_{\text{Raw gas}}$/kg · m^{-3}		0.01		
$\dot{V}$/m^3 · s^{-1}		$5.9 \cdot 10^{-5}$		
K_1'/Pa · s · m^{-1}		$6 \cdot 10^3$		
K_2'/Pa · s · m · kg^{-1}		$96 \cdot 10^3$		

The calculations for the bottom filling and sidewall cake growth are based on a simple geometric model of a triangular model pleat with the length L. The model pleat, including all relevant geometric parameters, for both models is depicted in Fig. 7. Relevant data for modeling is listed in Table 3.

The model pleat has a sidewall length of s_0, a width of b_0 and an opening angle θ, both of which vary for different pleat ratios. The relevant parameters for calculating the differential pressure for the first model are the time (or dust mass) dependent parameters $s_{\text{p}}(\text{t})$ and $b_{\text{p}}(\text{t})$, where the index p denotes a plug, as the blocking dust inside the pleat bottom can be interpreted as a plug lodged into the pleat bottom. With increasing filtration time $s_{\text{p}}(\text{t})$ increases due to the growth of the plug and thus reduces the available filter medium surface area. The equations used for calculating the differential pressure rise are given below. A detailed derivation of the relevant equations can be found in Appendix A.

The differential pressure for the bottom filling model, which is influenced only by the filter media resistance K_1' and w_{Filter}, can be calculated with Eq. (1).

$$\Delta p_{\text{bottom filling}}(\text{t}) = K_1' \cdot \frac{\dot{V}}{2 \cdot L \cdot (s_0 - s_{\text{P}}(\text{t}))} \tag{1}$$

For the sidewall cake growth, which consists of a continuously growing dust cake on the sidewalls with the thickness $\tau(\text{t})$ and a non-permeable plug in the bottom of the pleat, as shown in Fig. 6, a different calculation is used. By definition the plug begins, where both the dust cakes on the sidewalls meet, indicated by the dotted red lines in Fig. 7. The differential pressure increase for the sidewall cake growth can be calculated by Eq. (2), where ρ_{eff} represents the bulk density [$\rho_{\text{eff}} = (1-\varepsilon)\cdot\rho$] and K_2' the specific cake resistance.

$$\Delta p_{\text{sidewall growth}}(\text{t}) = (K_1' + K_2' \cdot \tau(\text{t}) \cdot \rho_{\text{eff}}) \cdot \frac{\dot{V}}{2 \cdot L \cdot s_0 \cdot \left(1 - \frac{2\cdot\tau(\text{t})}{b_0}\right)} \tag{2}$$

Using the expressions for the differential pressure (Eqs. (1), (2)), a comparison with experimental data can be performed to evaluate the dust loading behavior of the pleats and potentially offer qualitative insights on dust loading mechanisms. The porosity of the dust cake was used as an adjustment parameter in the range of 0.6–0.8, as was found by Schmidt [2].

2.2.2. Irreversible loss of filter media surface area over numerous cycles due to dust deposition inside the pleats

The second model approach is the irreversible loss of filter media surface area due to deposited dust inside the filter medium pleats, which cannot be removed by regeneration, and thereby continuously blocks filter media surface area. It is important to note that in this consideration the exact location of the blocked surface area is irrelevant. The differential pressure of surface filters can be calculated according

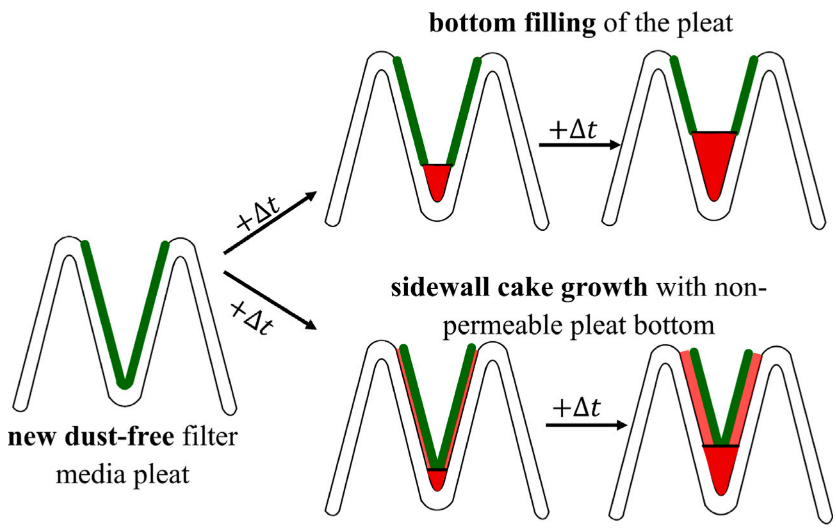

Fig. 6. Exemplary accumulation of dust inside the pleat for a bottom filling scenario and a continuous cake growth on the sidewall of the pleat with a non-permeable dust cake in the pleat bottom.

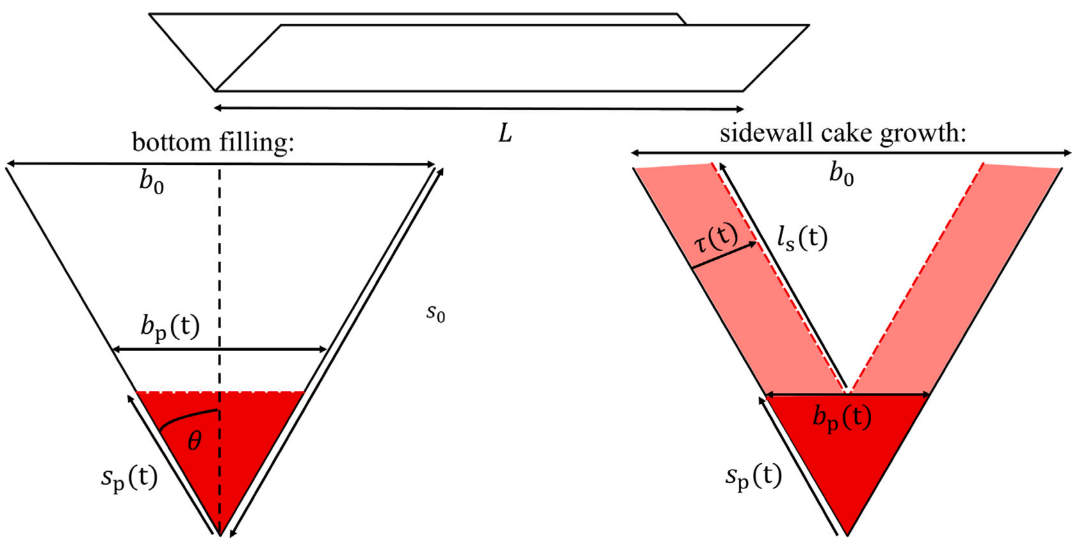

Fig. 7. Model pleat and relevant geometric parameters used in the bottom-filling and sidewall-cake-growth models.

to Löffler [1] by Eq. (3), where W represents the deposited areal dust mass.

$$\Delta p_{\text{Filter}} = K_1' \cdot w_{\text{Filter}} + K_2' \cdot w_{\text{Filter}} \cdot W \tag{3}$$

The filter media face velocity can be calculated using Eq. (4) and the areal dust mass over a certain time interval following Eq. (5), with t being the elapsed time since the last regeneration.

$$w_{\text{Filter}} = \frac{\dot{V}}{A_{\text{Filter}}} \tag{4}$$

$$W = \frac{\dot{V} \cdot c_{\text{Raw gas}} \cdot t}{A_{\text{Filter}}} \tag{5}$$

Exemplary calculated differential pressure curves for the different aging and surface area blocking scenarios are depicted in Fig. 8. Four different mechanisms are shown. The differential pressure curve for the non-aged filter medium increases over time, while the available surface area (indicated in green) is completely accessible and no dust has deposited inside the filter medium. For an aged filter medium, the deposited dust inside the filter media is indicated by the dotted red lines beneath the available surface area. If the filter medium ages the resistance K_1' increases. When this is the case the differential pressure curve depicts a y-axis intercept on a higher differential pressure level. When no blocked area occurs the curve will be shifted parallel to the higher differential pressure level, but with the same slope as the new, non-aged media during the filtration cycle.

If filter medium surface area is blocked by dust (and thus, impermeable), as indicated by the red areas in the pictograms above and besides the curves in Fig. 8, the differential pressure curves vary from the non-blocked filter medium. For the calculation of the curves (parameters are given in Fig. 8) the effective surface area was reduced by 40%. The reduction of surface area in combination with a constant volumetric flow results in an increase of w_{Filter}. This leads to a steeper differential pressure increase and a higher starting differential pressure. If, in addition to the loss of effective filter medium surface area, the medium is aged, the initial differential pressure increases further, but the slope of the differential pressure curve is equivalent to the slope with blocked filter medium surface area with a non-aged media with the same blocked surface area.

To evaluate potential filter medium aging and the blocking of effective/active surface area, the rise in differential pressure is used. For a set time interval Δt two points (at the beginning and the end of the

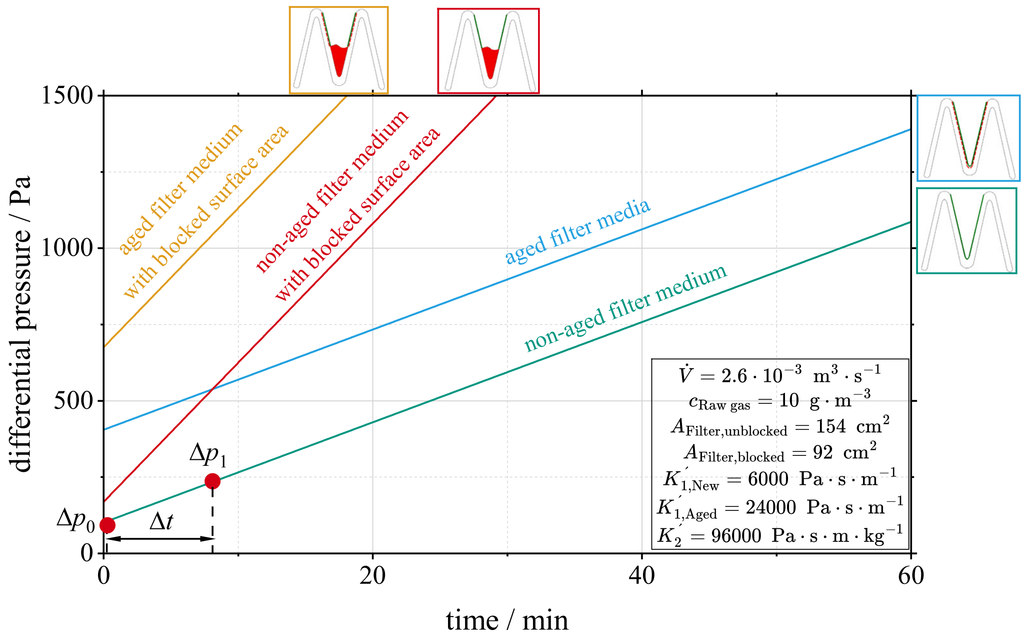

Fig. 8. Exemplary calculated differential pressure curves for differently aged filter media and effective surface area blocking scenarios.

interval) for the differential pressure are extracted and the application of Eqs. (3) and (5) results in Eq. (6). For the model consideration no dust is deposited inside the filter medium during one filtration cycle, resulting in a constant K'_1 during each filtration cycle.

$$\frac{\Delta p_1 - \Delta p_0}{t_2 - t_1} = \frac{\Delta(\Delta p)_{New}}{\Delta t} = K'_2 \cdot w_{Filter} \cdot \frac{\dot{V} \cdot c_{Raw\ gas}}{A_{Theoretical}} \tag{6}$$

Similarly the same procedure can be conducted for the aged stage of the filter medium, resulting in Eq. (7).

$$\frac{\Delta p_1 - \Delta p_0}{t_2 - t_1} = \frac{\Delta(\Delta p)_{Aged}}{\Delta t} = K'_2 \cdot w_{Filter} \cdot \frac{\dot{V} \cdot c_{Raw\ gas}}{A_{Effective}} \tag{7}$$

Forming the quotient and applying Eq. (4) yields Eq. (8). If this is rearranged and the new, unblocked filter medium surface area $A_{Theoretical}$ is interpreted as the total theoretical filter medium surface area and $A_{Effective}$ represents the available effective filter media surface area of the aged or potentially blocked filter medium, the potential loss of surface area can be quantified by Eq. (9).

$$\frac{\Delta(\Delta p)_{New}}{\Delta(\Delta p)_{Aged}} = \frac{\frac{\dot{V}}{A_{Theoretical}} \cdot \frac{1}{A_{Theoretical}}}{\frac{\dot{V}}{A_{Effective}} \cdot \frac{1}{A_{Effective}}} \tag{8}$$

By applying Eq. (9) a factor for the loss of filter media surface area can be calculated using differential pressure data gained by experiments. This approach enables indirect quantification of effective filter medium surface area using measurable differential pressure data. Furthermore, it offers insight on the mechanisms of permanent dust accumulation occurring during the experiment.

$$\frac{A_{Effective}}{A_{Theoretical}} = \sqrt{\frac{\Delta(\Delta p)_{New}}{\Delta(\Delta p)_{Aged}}} \tag{9}$$

3. Results and discussion

To characterize the impact of different filter medium geometries on the operating behavior the methodology described in Section 2.1.5 was applied. The following section will address the different stages of the methodology. Each geometry was tested three times except PR3, which was tested twice. Mean values were calculated from the available experiments. Consequently, the statistical reliability of the PR3 results is slightly lower than for the remaining geometries.

3.1. Conditioning cycles for different filter media geometries

The conditioning phase is conducted to evaluate the behavior of new, unused filter media. To eliminate ramp-up effects of the dust feeder, the raw gas concentration was first set in the raw gas duct, before initiating the flow through the filter media. This enables the evaluation of the initial particle penetration through the filter media under identical experimental conditions at the media face for each geometry.

Fig. 9 depicts the rise of the differential pressure during the first conditioning cycle for each medium geometry (left) and the initial particle penetration, represented by the particle number concentration measured on the clean gas side, through the filter media on the right. The differential pressure curves are representative raw-data curves from individual experiments. The particle number concentration shown represents the mean number concentration for the conducted experiments for each filter media geometry during the first cycle. Standard deviation from the mean is indicated by the shaded (lightly colored) areas. This depiction was chosen throughout this study, if error bars would reduce readability of the figures.

At the beginning of the cycle the increase of differential pressure is similar for all geometries, reflecting the harmonized operating conditions. The flat geometry (PR0) shows a decreasing differential pressure curve over time, whereas the pleated geometries exhibit a similar behavior up to approximately 5 min. Beyond this point PR2 and PR3 depict an almost linear increase in differential pressure, whilst PR4 and PR5 show an accelerated (non-linear) increase. This indicates a geometry- and time-dependent difference in differential pressure rise during dust loading, affecting the cycle time until the maximum allowed differential pressure is reached. For the pleated geometries a simple geometrical model was developed to describe and evaluate this behavior (Section 2.2.1). The decreasing slope for the flat filter medium (PR0), especially in the first cycle, suggests a non-homogeneous membrane laminated on the surface of the fibers. This can lead to non-uniform flow through the filter medium, an inhomogeneous cake build-up and a non-linear differential pressure rise with a decreasing slope, as the flow homogenizes during cake build-up.

The particle number concentration (Fig. 9) also varies for the different geometries. PR3 and PR4 exhibit the highest peak concentration of 3370 particles cm^{-3} and 2025 particles cm^{-3} respectively. Furthermore,

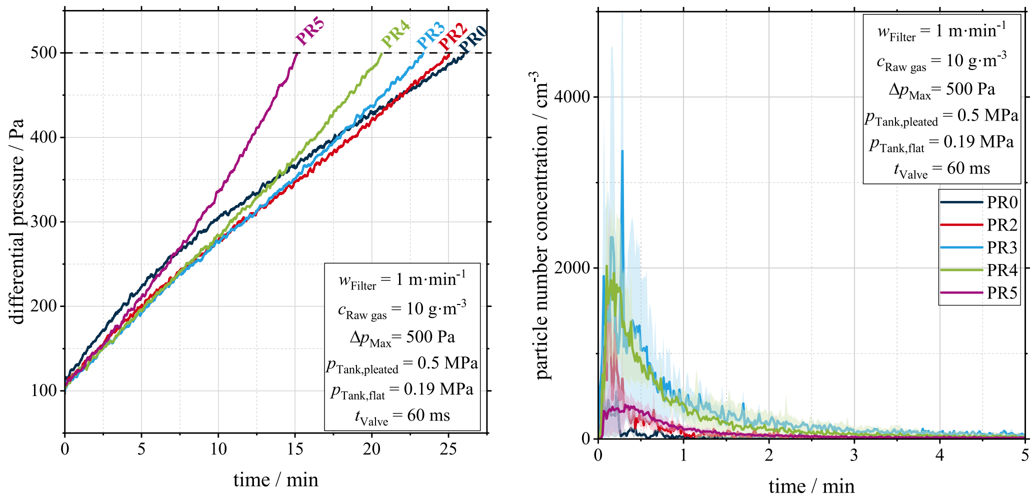

Fig. 9. Experimental differential pressure increase of the new, non-aged filter medium during a representative filtration cycle (left) and the mean particle number concentration during the first particle penetration through the filter medium (right), where the shaded areas represent standard deviation.

these two geometries emit particles for the longest, before reaching a near-zero particle number concentration after about 3–4 min. PR0 and PR5 exhibit a maximum of 560 particles cm^{-3} and 400 particles cm^{-3}, and show a decrease to a near-zero concentration after 1–2 min. PR2 shows intermediate behavior, but exhibits a similar trend in particle number concentration decay as PR0 and PR5. Since no residual dust cake is present during the first cycle, the emission behavior can be directly attributed to filter geometry and the resulting dust deposition patterns.

A possible explanation is that PR0 promotes homogeneous dust cake build-up, and in combination with the ePTFE membrane on the upstream side this results in a short emission event, with a low emission level. PR2 has very wide pleats, which lead to a low inlet velocity into the pleats and allows the formation of a homogeneous dust cake on the sidewalls and inside the pleat bottom. As the geometry is not completely flat, the resulting emission level is higher, compared to PR0, but shows the same, fast decrease to a near-zero emission level. For increasing PR the inlet velocity into the pleats increases and the particles cannot follow the streamlines towards the filter medium, resulting in the deposition of larger particles into the pleat bottom, while small particles mainly penetrate through the sidewalls of the pleats, before the dust cake is formed. This inhomogeneous cake build-up results in a higher emission level and a longer emission duration for PR3 and PR4. This effect should lead to the highest emission levels for PR5, as the highest pleated geometry. It can be seen that this is not the case. This could be due to the faster, temporal pleat filling with dust, due to the narrow pleat. As the test dust was free-flowing an optical evaluation of the formed dust cake is not possible, as the dust flows out of the pleats if the holder is disassembled offline after testing.

Applying the model calculations introduced in Section 2.2.1 results in the differential pressure curves shown in Fig. 10 for a new, non-aged filter media. The experimental data curves for PR2 and PR5 are shown for illustrative purposes to assist with interpretation, as these geometries represent the least (excluding PR0) and highest pleated geometry. On the left the calculations for the bottom filling are depicted, where the increase in filter media face velocity and the filter media resistance are dominant for the differential pressure increase. The bottom filling as a deposition pattern underestimates the experimental results, leading to the conclusion that omitting the influence of the dust cake above the plug at the pleat bottom is not correct and that dust also has to accumulate on the sidewalls of the pleats. The dust cake on the sidewall has to be considered, as is the case for the model with continuous dust cake growth on the sidewalls. The differential pressure curves for sidewall cake growth are shown in Fig. 10 on the right. It is shown that the experimental data act as an envelope for the modeled differential pressure curves. This suggests that considering the dust cake on the pleat sidewalls and reducing the effective filtration area by assuming the -smaller- dust plug in the pleat bottom better represents the experimental data and thus will be considered further.

For further evaluation of the sidewall cake build-up the differential pressure for the dust cake porosity of 0.6 and 0.8 was calculated, to create an envelope for a relevant porosity range of the dust cake in regards to surface filtration [2]. The results for the differently pleated filter media geometries are shown in Fig. 11. The model is in good accordance with the experimental data for all geometries for the first 7.5 min. This can indirectly indicate that the initial dust cake deposition inside the pleat is a combination of a dust cake forming on the sidewalls of the pleats and a small amount of dust accumulated in the pleat bottom. As the dust cake on the sidewalls is not very thick in the beginning of the cycle, the blocked area in the pleat bottom is small and most of the pleat area is effective filtrater media surface area. For PR2 and PR3 the model overestimates the differential pressure increase after the initial 10 min. The qualitative trend of differential pressure increase for PR4 and PR5 is represented well.

As the models, based on a simple, triangular geometry, do not consider effects such as compression of the dust cake and filter media, deposition of particles inside the filter media, the permeability of the plug in the pleat bottom and the resulting influences on the differential pressure increase, only qualitative insights can be drawn from the modeling results.

Nevertheless, the model qualitatively represents the experimental data, especially for PR4 and PR5, and is consistent with the assumption that dust deposits on both the pleat sidewalls and in the pleat bottom. Furthermore, the combined experimental and modeling results suggest a direct influence of pleat geometry on the dust loading behavior. A narrower pleat distance leads to a steeper increase in differential pressure, which results in shorter cycles (Δp-controlled), even under the same experimental conditions and during the first cycle, where no previously deposited dust and patchy cleaning can influence the differential pressure evolution. As a result, the cycle time decreases for PR4 and PR5, as shown in Fig. 12. The results of the experimental data and the model calculations are also in accordance to more extensive numerical investigations that show an increasing differential pressure during dust loading for a higher pleat ratio [15,17]. Furthermore, experimental studies for both surface and depth filters show the same qualitative trend of an increasing differential pressure for a higher pleat ratio during dust loading already in the first cycle [30,31,51]. In addition, Teng et al. [27] showed that under the same dust mass

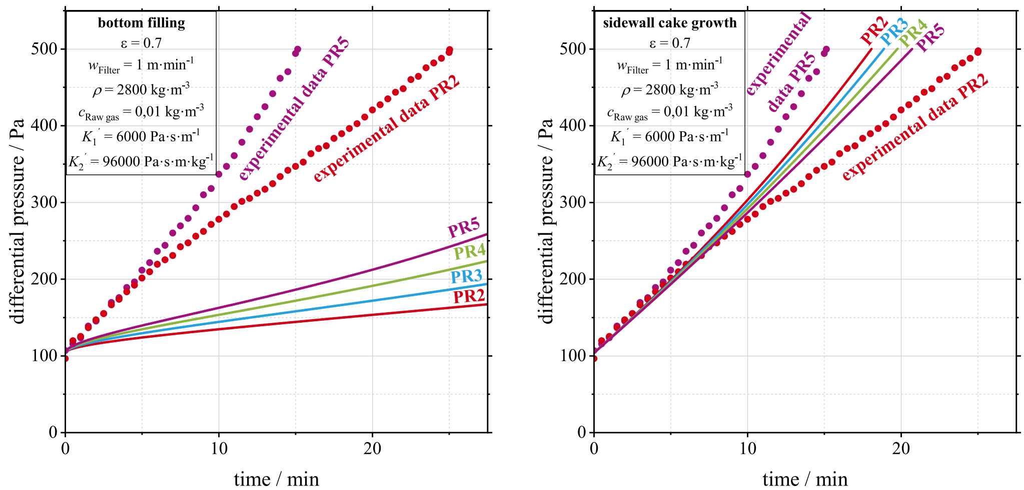

Fig. 10. Model calculations for bottom filling (left) and sidewall cake growth (right) for differently pleated filter media geometries (PR0 excluded, as the geometry is not pleated) and representative differential pressure curves for PR2 and PR5.

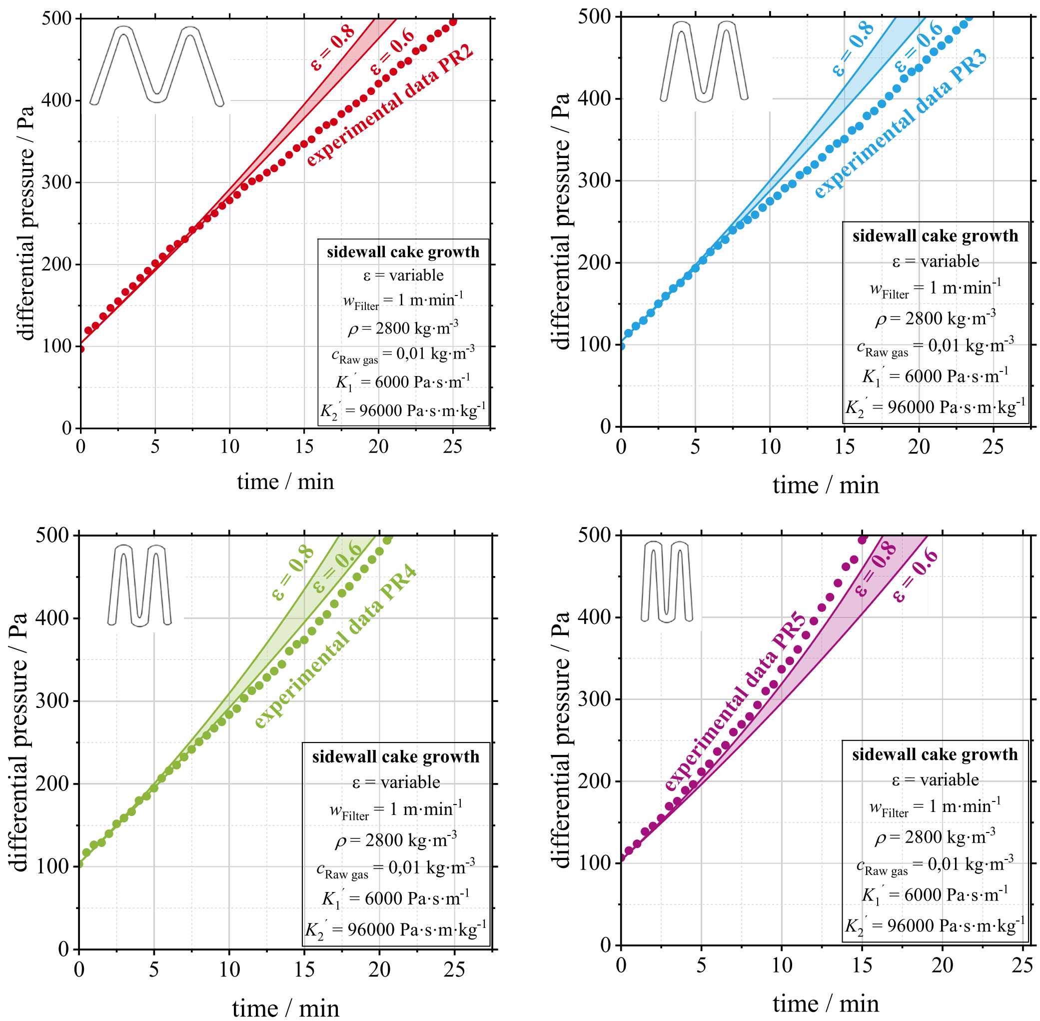

Fig. 11. Representative experimental data and the modeled envelope for dust cake porosities of 0.6 and 0.8 of the differential pressure for PR2, PR3, PR4, and PR5.

deposited per unit area for different filters, a higher PR results in a higher differential pressure. These findings support the proposed hypothesis that the time-dependent dust deposition within the pleats is an important factor for the development of differential pressure.

The development of the cycle time (left) and the residual differential pressure (right) for the conditioning cycles are shown in Fig. 12. The error bars represent standard deviation. In addition, the initial differential pressure for all filter medium geometries are shown on the

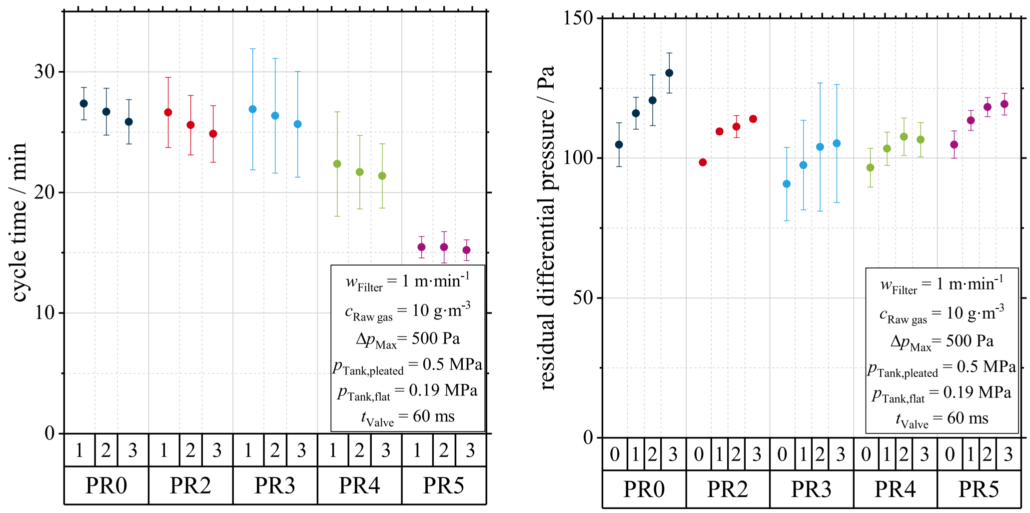

Fig. 12. Mean values and standard deviation for the development of the cycle time (left) and residual pressure development (right) for each conditioning cycle for every filter media geometry (PR0, PR2–PR5).

right under cycle 0. The cycle time decreases for all geometries for each cycle. The decrease amounts to 1.8 min for PR0 and PR2 and 1.0–1.3 min for PR3 and PR4 respectively. The lowest reduction in cycle time is observed for PR5, which decreases by only 0.25 min. The flat geometry (PR0), PR2, and PR3 show a similar trend in cycle time, both in terms of decrease and cycle duration. All three geometries start with a cycle time of approximately 26 min and end the conditioning phase with a cycle time of 25 min. In contrast, PR4 and PR5 exhibit shorter cycle times from the first cycle onward, with PR5 showing the shortest cycle duration of 15 min.

In contrast, the residual differential pressure (shown on the right) increases with each filtration cycle. This is attributed to an increasing particle deposition within the new filter medium. The geometries PR2–PR5 exhibit a differential pressure increase of 10–15 Pa over the conditioning cycles, indicating similar particle deposition behavior. The flat geometry (PR0), however, shows an increase of 25 Pa, resulting in the highest residual differential pressure after conditioning. This may be attributed to more complete removal of the dust cake of the flat geometry, allowing deeper particle penetration and deposition into the filter medium, which leads to a higher residual pressure during the first cycles.

The variation of the initial differential pressure between the different geometries is below 10%, with mean initial differential pressure of 99 Pa. Compared to the maximum allowed differential pressure of 500 Pa, only 2% of the usable differential pressure range is lost due to fluctuations in the resistance of the new filter media. Therefore, differences in initial differential pressure are neglected in the following analysis. These variations may arise from local inhomogeneities and minor damage to the filter medium or membrane during pleating and manufacturing of the filter element.

Not just the initial particle penetration in the beginning of the first cycle, shown in Fig. 9, but also the development of the particle emission over the conditioning cycles is an important evaluation criterion for the operating behavior. The average emission per cycle (from regeneration to the next regeneration) is depicted in Fig. 13. The average number concentration for the first cycle is the highest for each geometry and has the largest error bars, showing standard deviation. This is due to the first penetration of particles through the new filter media, with no particles deposited inside the media. Furthermore, by pleating the filter media and by implementing the media into the 3D-printed structure small defects to the membrane can occur, which result in a poorer particle collection in the first cycle. These defects can be compensated by particle deposition in the defect areas, but are not structurally quantifiable. As a result, the height of the initial particle penetration can vary. The subsequent cycles show a similar level of emissions, which is lower than in the first cycle due to particle deposition inside the filter media, with again PR0 and PR5 having the lowest average number concentration of 10–30 particles cm^{-3}. PR2–PR5 exhibit an average number concentration between 40–85 particles cm^{-3}.

3.2. Aging of the different filter media geometries

The second phase of the experimental procedure is the accelerated aging of the filter media. This phase is used to simulate long-term use of the filter media by regenerating the filter media in short successive intervals. This enhances particle deposition inside the filter media, resulting in an increasing filter media resistance and a better particle separation and lower particle emission, as particle penetration is reduced by the deposited particles.

The development of the differential pressure (left) and the particle number concentration (right) over the 500 aging cycles is shown in Fig. 14. One characteristic value was determined for each aging cycle. For the differential pressure the maximum differential pressure of each 30 s interval is chosen, as this correlates to the value directly before regeneration and quantifies the relevant increase of differential pressure. The curves represent the mean value of the three experiments conducted for each geometry, except for PR3, for which only two experiments were conducted. For the particle number concentration the mean value for each cycle is depicted to compensate the fluctuation in signals due to the measuring device.

The qualitative trend of differential pressure increase, shown in Fig. 14 on the left, is similar for all geometries. The differential pressure starts at 0 Pa, as the residual pressure after the conditioning phase was subtracted for each geometry for better comparison. After a steep increase of the differential pressure the curves level off after about 100 cycles. The further increase of differential pressure for all pleated geometries (PR2–PR5) is qualitatively the same, only on a slightly different level. The differential pressure of PR2–PR5 rises between 45–50 Pa, which can be attributed to minor differences in each filter media sample. Although PR0 exhibits a similar initial trend, the total increase during aging is higher (66 Pa). This can be the result of better dust cake detachment after each regeneration pulse, compared to the pleated geometries, which can benefit the particle deposition inside the filter media.

The particle number concentration in Fig. 14 on the right also depicts the same trend for all geometries. The emission level in the early stages of aging is high and then decreases over the successive aging cycles, as more particles are deposited inside the media and thus enhance

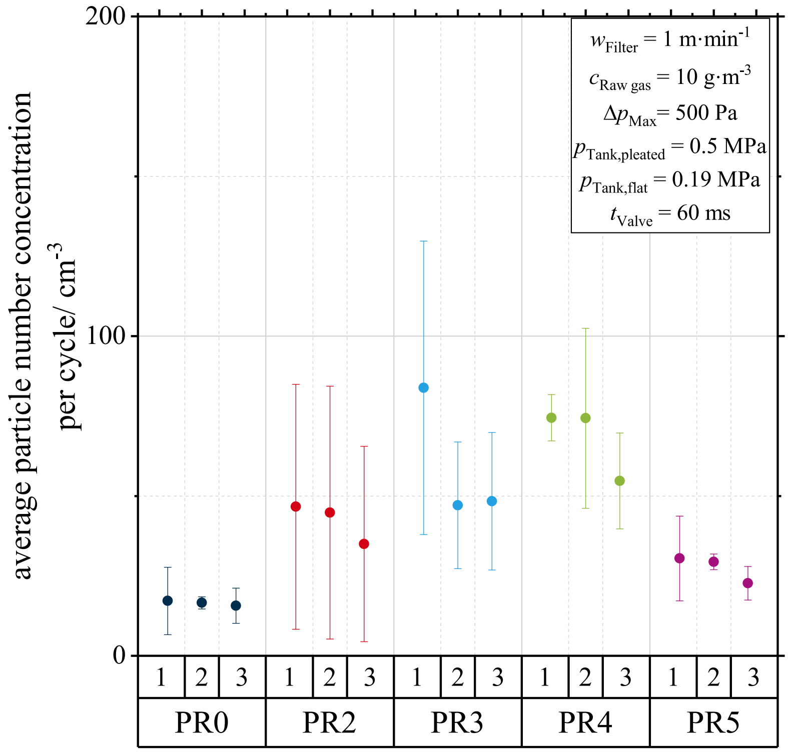

Fig. 13. Average particle number concentration and standard deviation per cycle from the conditioning phase of PR0 and PR2–PR5.

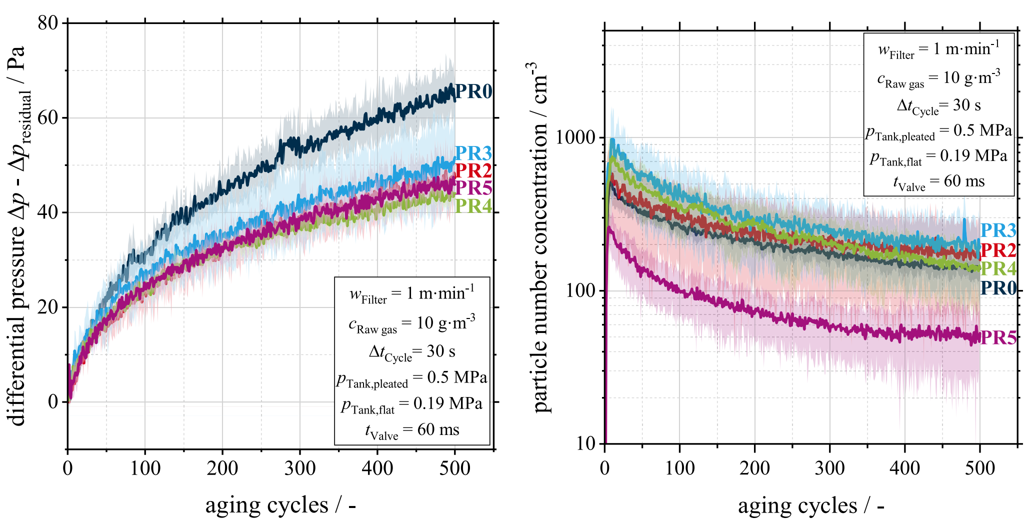

Fig. 14. Development of differential pressure (left) and particle number concentration (right) during the 500 Δt-controlled aging cycles. Solid lines represent the mean values of the experiments, and the shaded areas indicate the corresponding standard deviations.

the dust separation ability of the filter media. The overall emission levels correlate with the initial behavior shown in Fig. 9, where PR3 and PR4 emit the most particles followed by PR2. PR0 and PR5 exhibit the lowest emission level. Considering the ratio between the highest and lowest particle number concentration during aging, a reduction by a factor of approximately 4–5 is observed for all geometries. Since this reduction is similar across all cases, it can be concluded that the macroscopic aging, based on development of differential pressure and particle number concentration, is comparable. Therefore, differences in absolute emission levels are likely associated with geometry-dependent dust deposition patterns within the pleats.

Summarizing the aging phase, two aspects stand out. The increase in differential pressure for PR2–PR5 was similar, considering the fluctuations attributed to different filter media samples. The differential pressure increase for PR0 could likely be a result of a more thorough and uniform media aging. Furthermore, all geometries show a similar reduction in particle number concentration (factor of 4–5). Both of these aspects indicate a similar aging in respect to differential pressure increase and particle concentration reduction of all geometries. This suggests that the observed differences in differential pressure and the particle emission are the consequence of different media geometries and can already be seen in early stages of filter testing, as discussed in Section 3.1.

3.3. Measurement phase of differently pleated filter media

During the measurement phase, the cycle time, the residual differential pressure, and the average particle number concentration were

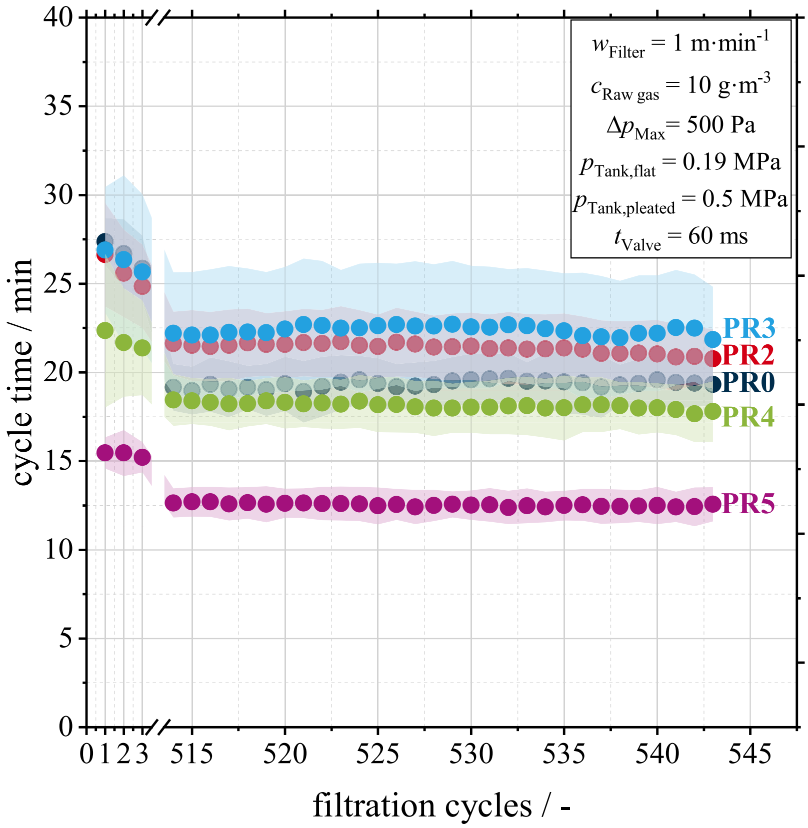

Fig. 15. Development of the mean cycle time during the conditioning and measurement cycles for PR0 and PR2—PR5. The shaded areas indicate the corresponding standard deviations.

evaluated to assess the operating behavior of the different filter media geometries.

3.3.1. Cycle time development during the measurement phase

Fig. 15 depicts the development of the cycle time for each considered geometry. The cycle time during the first three cycles (conditioning phase) is shown to emphasize the effect of aging the filter media. Again the shaded areas represent standard deviation for the mean values. The aging and stabilizing phase are omitted for the sake of clarity.

For all geometries three effects can be observed. The cycle time decreases for all geometries during conditioning (see Section 3.1). The aging reduces the cycle time as the filter media resistance increases which reduces the usable differential pressure range until the allowed differential pressure is reached. Thirdly, all geometries exhibit a stable operation behavior, as the cycle time does not increase over the successive measurement cycles. This indicates a consistent removal of dust cake and a stable residual differential pressure level. In contrast, an unstable operating behavior would result in a decrease of cycle time over successive cycles, due to an increasing residual differential pressure and a smaller differential pressure range before regeneration, when Δp – cycles are conducted. Furthermore, stable operation implies sufficient filter media aging applying the described procedure in Section 3.2.

PR0 ages the most during the aging phase, reaching a cycle time of 19 min during the measurement phase, and a decrease of 7.5 min compared to the first cycle. The cycle time for PR0 is decreased by 28% due to aging of the filter medium. As the pleated geometries age similarly during the second stage, the decrease of cycle time for all pleated variants (PR2–PR5) is 17%–18%.

Comparing the pleated geometries, (excluding PR0), the cycle time for PR5 is the shortest in average at 12 min, followed by PR4 with 18 min and then PR2 and PR3 with 21 min and 22 min. Again this qualitative order can be seen directly at the beginning of the first cycle and is consistent throughout the entire experiment. Nevertheless, evaluating different aging stages of the filter media offers further insights into the long term operating behavior.

3.3.2. Residual differential pressure development during the measurement phase

The development of residual differential pressure shown in Fig. 16 indicates stable operating behavior for all geometries. This observation is supported by the low coefficients of variation (CV) reported in Table 4. Again, standard deviation is shown by the shaded areas. The height of the residual differential pressure is a result of different filter media aging, if PR0 and PR2–PR5 are compared. The flat geometry ages the most if the differential pressure is considered, resulting in a residual differential pressure of 185 Pa, which is a 80 Pa increase from the new flat media. For the pleated geometries the slight differences in the initial differential pressure are mirrored in different levels of residual differential pressure. As the pleated geometries all exhibit similar aging behavior, the increase of differential pressure from the initial values of new samples results in a residual differential pressure level of 165 Pa for PR2 and PR5 after aging and stabilization, while PR3 and PR4 exhibit a residual pressure of about 152 Pa.

Notably, PR2 and PR5 exhibit similar residual differential pressure but significantly different cycle times (difference of approximately 9 min). This demonstrates that not only the residual differential pressure, but also the rate of differential pressure increase during a filtration cycle must be considered when evaluating filter performance.

This observation confirms that the pleat geometry can strongly influences the development of differential pressure, as previously discussed in Section 3.1. The results for the cycle time and the residual differential pressure are summarized in Table 4 as mean values ±

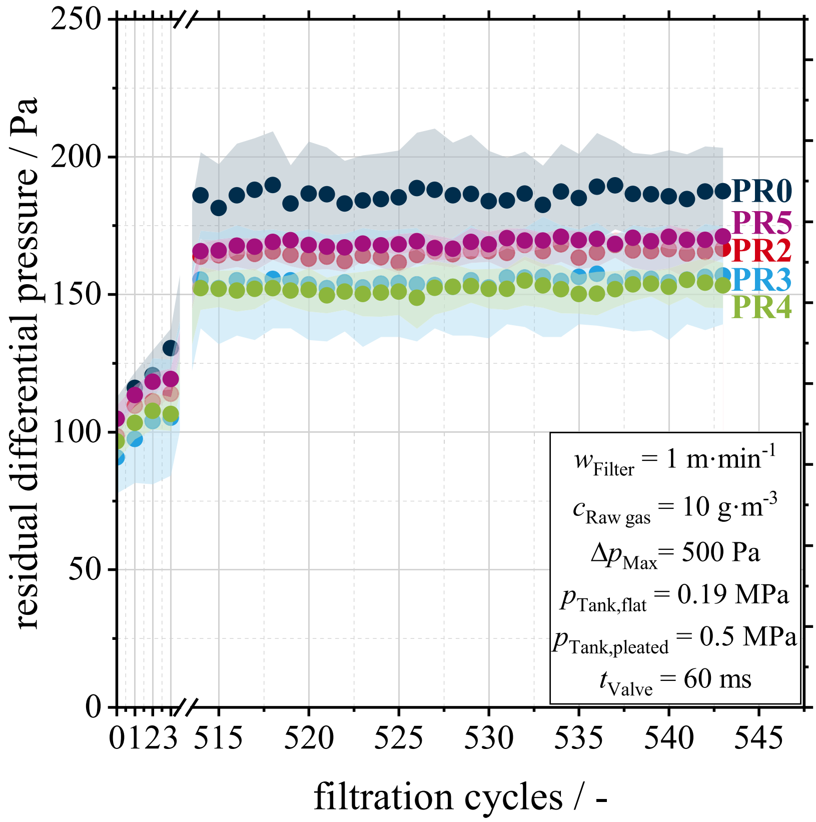

Fig. 16. Mean values and standard deviation as shaded areas of the development of the residual differential pressure during the conditioning and measurement cycles for PR0 and PR2–PR5.

Table 4
Summary of the mean residual differential pressure and the cycle time for the measurement cycles with standard deviation.

	Measurement cycles			
	Residual differential pressure/Pa	CV/%	Cycle time/min	CV/%
PR0	185.99 ± 2.09	1.12	19.33 ± 1.44	1.03
PR2	165.02 ± 1.56	0.95	21.38 ± 1.89	1.23
PR3	154.73 ± 1.46	0.95	22.39 ± 3.43	1.12
PR4	152.06 ± 1.52	1.00	18.13 ± 1.48	0.99
PR5	168.75 ± 1.50	0.89	12.53 ± 0.92	0.70

Table 5
Mean differential pressure rise during the conditioning and measurement cycles.

	Differential pressure rise/Pa · min^{-1}	
	1st conditioning cycle	1st measurement cycle
PR0	22.33 ± 1.29	22.76 ± 0.56
PR2	19.61 ± 3.99	16.62 ± 2.90
PR3	17.22 ± 2.86	15.45 ± 2.14
PR4	16.70 ± 1.25	17.29 ± 2.55
PR5	20.82 ± 0.57	23.71 ± 1.55

standard deviations based on three experiments for PR0, PR2, PR4, and PR5 and two experiments for PR3. Furthermore, the CV is shown as a stability metric for the residual differential pressure and cycle time.

3.3.3. Loss of filter media surface area due to dust deposition inside the pleats

To evaluate the loss of effective filtration area due to permanent blocking of surface area by dust, the model described in Section 2.2.2 was applied. Fig. 17 depicts exemplary, raw-data differential pressure curves for the first conditioning and the first measurement cycle for each filter media geometry. These cycles are selected, as they represent the new, unused filter media in the beginning and the filter media after aging and stabilization. To obtain the necessary data to apply Eq. (9), the differential pressure at the start and the end of a two minute interval was determined, as indicated by the turquoise arrows in Fig. 17. The interval for data collection was set at the beginning of the respective filtration cycle (minute 2 and 3). At beginning of the cycle effects on the differential pressure development, such as patchy cleaning or surface area loss, are most prominent.

All filter media geometries show the same qualitative behavior. The differential pressure curve of the conditioning cycle starts around 100 Pa for all geometries. After the aging and stabilization all geometries exhibit a higher starting differential pressure, as discussed in Section 3.2. If the available filter media surface decreases, the slope of the differential pressure curve during the measurement cycle would rise steeper compared to the slope of the new, unused filter media under identical experimental conditions. The evaluation of the ratio between effective and theoretical filter media surface area shows that for PR0 and PR2–PR4, aging does not lead to a noteworthy reduction in effective surface area, as the ratio remains close to unity. PR5 shows a slight decrease of approximately 6% of effective filter media surface area in the chosen interval. The differential pressure increase rate for the different geometries are summarized in Table 5.

This indicates that, with the same specific regeneration intensity, harmonized experimental parameters, and the coarse, free-flowing dust, the permanent loss of effective filter media surface area is negligible, as the differential pressure rise for the new and aged filter media is almost similar, with a slight decrease noticeable for PR5. This can be attributed to the good dust cake removal of the free-flowing dust under the chosen regeneration intensity (maximum peak pressure), which leads to no occurrence of significant blocking inside the pleats. Kim

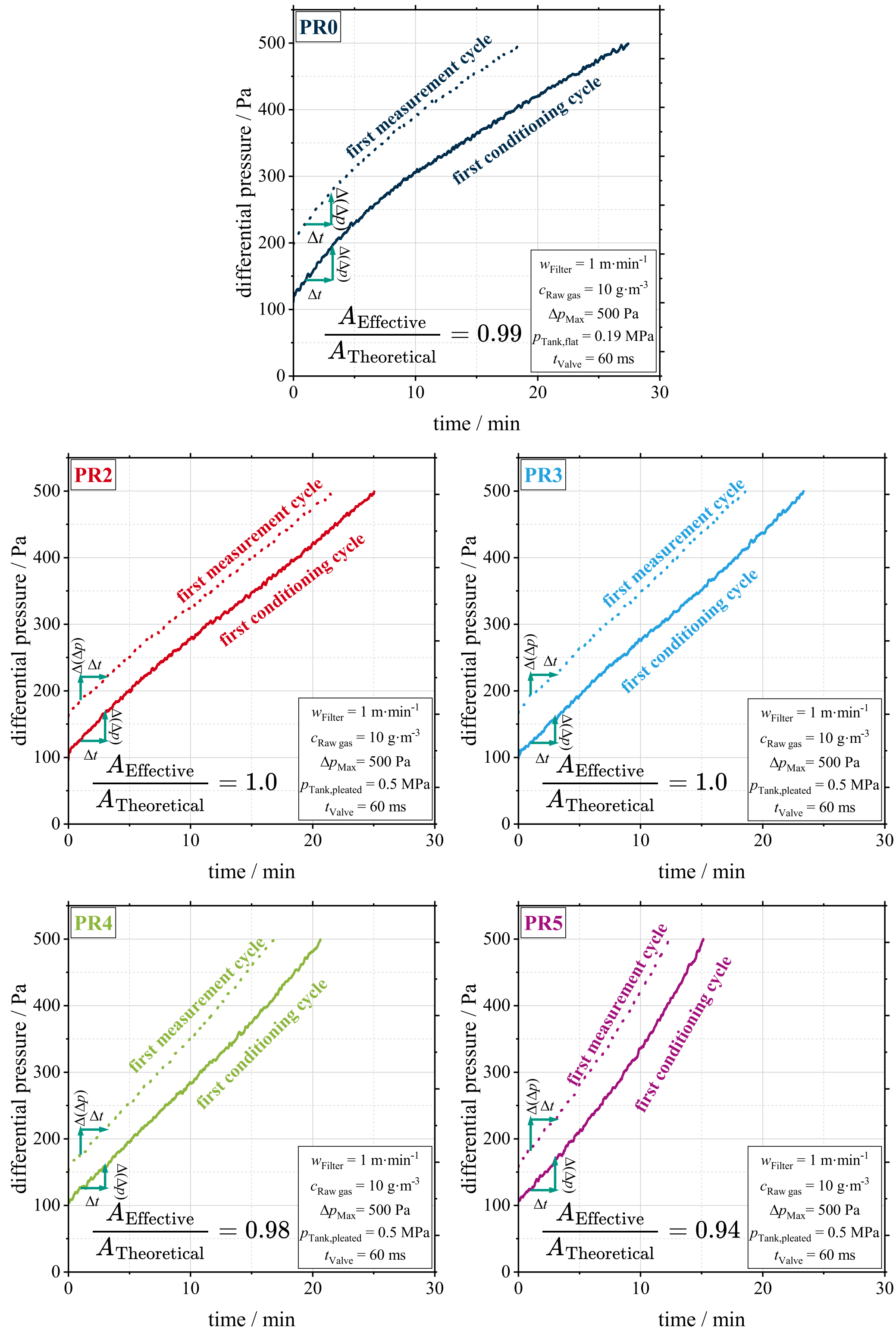

Fig. 17. Comparison of the differential pressure increase of representative experiments for the first conditioning and measurement cycle of each geometry to evaluate potential filter media surface area loss due to permanent blocking.

et al. [25] and Cuiping et al. [28] attributed a decreasing cycle time to a higher pleat ratio. The higher pleated filter elements in these studies exhibited a varying filter media surface area, but the tank pressure was 0.4 MPa for all experiments, resulting in a differing maximum peak pressure for the different filter elements during regeneration. A lower intensity of regeneration results in a differing dust cake removal for

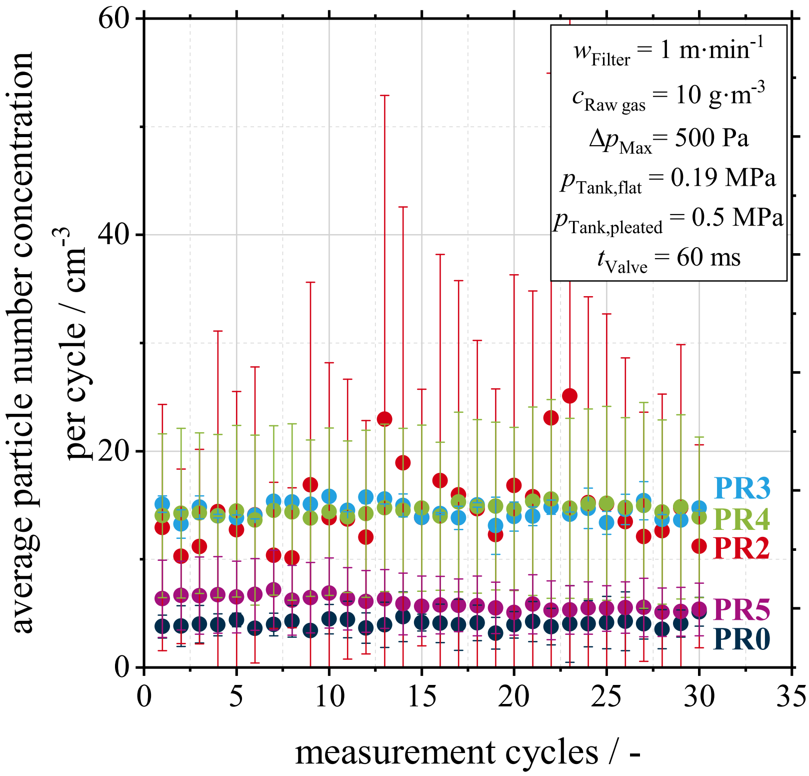

Fig. 18. Average particle number concentration and standard deviation for each measurement cycle for PR0 and PR2–PR5 measured with a WELAS 2300 sensor (set size range: 0.2–10 μm).

the different pleated elements. This makes it difficult to assess the sole impact of filter media geometry on effective surface area loss.

3.3.4. Average particle number concentration during the measurement phase

The average particle number concentration per cycle, shown in Fig. 18, exhibit the same qualitative trend discussed in Section 3.1. PR0 and PR5 exhibit the lowest average particle number concentration of approximately 4–6 particles cm^{-3}. For the used sensor these values correlate to the count rates of 2–3 particles per second on average on the clean gas side. The low emission level shows the qualitative trend depicted during the conditioning cycles.

The geometries between the flat and PR5 (PR2–PR4) exhibit the same particle number concentration of 15 particles cm^{-3}, resulting in a 2.5-times higher emission level than PR0 and PR5. This is primarily due to higher peak particle emissions during regeneration and longer emission durations before reaching near-zero concentration, as discussed previously.

4. Conclusion and outlook

The main contribution of this work is the isolated evaluation of the influence of pleat geometry (spacing) on the operating behavior of cleanable surface filters under harmonized operating and regeneration conditions. The investigation was conducted using one ePTFE-laminated PES filter medium, one filter face velocity, one harmonized regeneration setting, and a coarse, free-flowing Boehmite test dust. An adapted DIN ISO 11057 procedure enabled the measurement of geometry effects while maintaining identical operating and regeneration conditions for all investigated pleat geometries. Furthermore, a simple modeling approach was used to assess the potential loss of effective filter media surface area during dust loading.

The results demonstrate that the filter medium geometry influences operating behavior from the initial conditioning cycles onward. Differences in differential pressure, cycle time, and particle emission are established immediately and persist throughout operation. Increasing the pleat ratio resulted in shorter filtration cycles, but no pronounced geometry-depended influence on the residual differential pressure was observed under the investigated conditions. The comparison with the flat reference geometry, with harmonized operating conditions at the filter media face, revealed the same general trend, although the flat geometry differs in filter media surface area and holder configuration.

The cycle time in particular depends on the pleat geometry, as a higher PR results in shorter cycles: The observed differential pressure development is consistent with the proposed deposition mechanism, in which particles accumulate on the pleat sidewalls and in the pleat bottom. According to the sidewall cake growth model, narrow pleats reduce the effective filter media surface area with growing mass deposition within a filtration cycle, leading to a reversible reduction of effective filtration area and an accelerated increase in differential pressure.

The observed aging behavior was comparable for all investigated pleat geometries, indicated by similar increases in differential pressure and decreases in particle number concentration during the accelerated aging procedure. Only the flat filter medium exhibited a slightly larger increase in differential pressure.

The comparison of cycles from before and after the aging phase to evaluate the potential surface area loss shows that no significant loss of effective filter media surface area occurs when regeneration intensity is properly adapted for the experimental parameters and test dust used in this study. This finding contrasts with previous studies reporting surface loss in pleated filter elements and suggests that such effects may result from insufficiently aligned regeneration conditions and differing test dusts, rather than pleat geometry.

The presented methodology enables the isolated evaluation of pleat geometry under harmonized operating and regeneration conditions. Under these conditions, it is shown that increasing the pleat ratio did not necessarily improve filter performance and resulted in shorter filtration cycles. However, the present results were obtained for defined operating parameters, one filter medium and one test dust. Consequently, direct engineering recommendations for industrial filter cartridges cannot yet be derived.

Future studies should extend the presented methodology to different filter media, dust types, operating conditions, and eventually filter cartridges to evaluate the effect of pleat geometry on relevant operating parameters such as differential pressure, cycle time, and particle emission. Furthermore, the effect of different regeneration parameters, such as tank pressure and valve opening time should be considered to deepen the under-standing of pleated filter elements and the effect of geometry on the operating behavior further.

CRediT authorship contribution statement

Jakob Paul Knisley: Writing – original draft, Data curation, Conceptualization, Investigation, Methodology, Visualization, Validation. **Julian Martin Schlegel:** Data curation, Investigation. **Jörg Meyer:** Writing – review & editing, Formal analysis, Conceptualization. **Achim Dittler:** Writing – review & editing, Supervision, Resources, Funding acquisition, Conceptualization.

Declaration of Generative AI and AI-assisted technologies in the writing process

During the preparation of this manuscript, the authors used ChatGPT 5 (OpenAI) to improve language clarity and readability. All scientific content, interpretations and conclusions were produced and verified by the authors. The authors take full responsibility for the accuracy and integrity of the work.

Declaration of competing interest

The authors declare that they have no known competing financial interests or personal relationships that could have appeared to influence the work reported in this paper.

Acknowledgments

We acknowledge the financial support and the close cooperation of the Filterkonsortium at KIT. The Filterkonsortium at KIT unites leading companies in the fields of fiber and media production, assembly, plant engineering and measurement technology with the research activities of the research group Gas–Particle-Systems of the Institute of Mechanical Process Engineering and Mechanics (MVM). The members of Filterkonsortium at KIT are as follows: BWF Tec GmbH & Co. KG, BWF Envirotec, ESTA Apparatebau GmbH & Co. KG, Freudenberg Filtration Technologies GmbH & Co. KG, Junker-Filter GmbH, MANN+HUMMEL GmbH, and Palas GmbH. Parts of this work were presented at FILTECH 2026.

Appendix A. Geometrical model of a pleated filter

The Appendix A is used to give detailed information on how the equations in Section 2.2.1 were derived and what model assumptions were made.

Model Assumptions

The following assumptions are applied to both models:

- The pleat is represented by a two-dimensional V-shaped geometry.
- Both flanks have identical length s_0 and enclose a symmetric opening width b_0, which varies for the different geometries.
- The pleat is extruded uniformly over a depth L.
- Dust is deposited homogeneously along the pleat depth L.
- The dust cake is characterized by the bulk density ρ_{eff}.
- The gas flow is assumed to remain constant and to be evenly distributed across the available filtration area.

The total clean filter area of the model pleat is

$$A_0 = 2 \cdot L \cdot s_0 \tag{A.1}$$

The horizontal distance $d_h(s)$ between the flanks at position s is

$$d_h(s) = \frac{b_0}{s_0} \cdot s \tag{A.2}$$

Bottom Filling

Additional assumptions

- Dust accumulates exclusively in the pleat bottom.
- No dust cake forms on the filter flanks.
- The plug is impermeable to flow.
- The plug forms a triangular shape in cross-section and increases over time.

Geometrical approximation

The plug length s_P is defined along the pleat flank. The vertical plug height h_P is related to the flank length by

$$h_P = s_P \cdot \cos(\theta) \tag{A.3}$$

For the pleat geometries in this contribution, the inclination angle θ (shown schematically in Fig. 7) is small. Therefore,

$$\cos(\theta) \approx 1 \tag{A.4}$$

and consequently

$$h_P \approx s_P \tag{A.5}$$

This approximation is used throughout the model. The small pleat angles result in only in minor deviations from the exact and simplified geometry between 0.5%–3% for the different pleat openings b_0.

Plug geometry

The width of the plug top surface is calculated with:

$$b_P(t) = \frac{b_0}{s_0} \cdot s_P(t) \tag{A.6}$$

The cross-section of the triangular plug is:

$$A_P = \frac{b_0}{2s_0} \cdot s_P^2(t) \tag{A.7}$$

Plug volume and deposited mass

$$V_P = \frac{b_0}{2s_0} \cdot L \cdot s_P^2(t) \tag{A.8}$$

$$m_P(t) = \rho_{eff} \cdot V_P \tag{A.9}$$

Plug growth during dust loading

$$m_P(t) = \dot{V} \cdot c_{Raw\ gas} \cdot t \tag{A.10}$$

By rearranging Eqs. (A.8) and (A.9) $s_P(t)$ can be calculated.

$$s_P(t) = \sqrt{\frac{2 \cdot s_0 \cdot m_P(t)}{\rho_{Eff} \cdot b_0 \cdot L}} \tag{A.11}$$

Effective filter media surface area

$$A_{Effctive} = 2 \cdot L \cdot (s_0 - s_P(t)) \tag{A.12}$$

Filter media face velocity and pressure drop

$$w_{Filter} = \frac{\dot{V}}{A_{eff}} \tag{A.13}$$

Following Eq. (3) and the assumption that only the free surface area $A_{\text{Effective}}$ is used for the volumetric flow, the differential pressure for bottom filling can be calculated by:

$$\Delta p = K_1' \cdot w_{\text{Filter}} \tag{A.14}$$

Continuous cake growth on the sidewalls with plug formation

Additional assumptions

- Dust is deposited uniformly on both pleat sidewalls (more specific, the fraction of the sidewall that is not blocked by a dust plug at the pleat bottom).
- The cake grows symmetrically with a uniform thickness $\tau(\mathrm{t})$ on both sidewalls.
- The plug forms when both cake layers intersect and is impermeable to flow.

Geometrical approximation

The cake thickness $\tau(\mathrm{t})$ is defined in horizontal direction for simplicity. For small pleat angles, this description is approximately equivalent for cake growth in horizontal direction and orthogonal to the media surface. Due to the small opening angles the error introduced between the exact and simplified cake thickness is between 0,5%–3% and thus neglected for the model calculations.

Plug formation in the pleat bottom

The plug is formed, when the dust cakes on both sidewalls meet, and as a result close the pleat bottom.

$$d_h(s) = 2 \cdot \tau(\mathrm{t}) \tag{A.15}$$

With Eq. (A.6) the covered sidewall length $s_{\mathrm{P}}(\mathrm{t})$ can be calculated with:

$$s_{\mathrm{P}}(\mathrm{t}) = \frac{2\tau(\mathrm{t}) \cdot s_0}{b_0} \tag{A.16}$$

Effective area

$$A_{\text{Effective}} = 2 \cdot L \cdot s_0 \left(1 - \frac{2 \cdot \tau(\mathrm{t})}{b_0}\right) \tag{A.17}$$

Mass balance

The entire mass inside the pleat is the sum of the mass on the sidewalls (flanks m_{F}) and inside the plug (m_{P}):

$$m(\mathrm{t}) = m_{\mathrm{F}}(\mathrm{t}) + m_{\mathrm{P}}(\mathrm{t}) \tag{A.18}$$

Cake build-up on the sidewalls of the pleat

$$V_{\mathrm{F}} = 2 \cdot \tau(\mathrm{t}) \cdot L \cdot s_0 \left(1 - \frac{2 \cdot \tau(\mathrm{t})}{b_0}\right) \tag{A.19}$$

$$m_{\mathrm{F}}(\mathrm{t}) = \rho_{\mathrm{eff}} V_{\mathrm{F}} \tag{A.20}$$

Dust deposition in the pleat bottom (plug build-up)

$$V_{\mathrm{P}} = \frac{2 \cdot L \cdot s_0}{b_0} \tau^2(\mathrm{t}) \tag{A.21}$$

$$m_{\mathrm{P}}(\mathrm{t}) = \rho_{\mathrm{Eff}} V_{\mathrm{P}} \tag{A.22}$$

Total mass deposited inside the pleat

Using Eq. (A.18) and rearranging results in the following for the entire mass inside the pleat

$$m(\mathrm{t}) = 2 \cdot \rho_{\mathrm{Eff}} \cdot L \cdot s_0 \left(\tau(\mathrm{t}) - \frac{\tau^2(\mathrm{t})}{b_0}\right) \tag{A.23}$$

Cake thickness on the sidewalls

Rearranging Eq. (A.23) leads to the cake thickness on the sidewalls

$$\tau(\mathrm{t}) = \frac{b_0}{2}\left(1 - \sqrt{1 - \frac{2 \cdot m(\mathrm{t})}{\rho_{\mathrm{Eff}} \cdot L \cdot s_0 \cdot b_0}}\right) \tag{A.24}$$

With the entire deposited mass inside the pleat the cake thickness results in

$$\tau(\mathrm{t}) = \frac{b_0}{2}\left(1 - \sqrt{1 - \frac{2 \cdot \dot{V} c_{\text{Raw gas}} \cdot t}{\rho_{\mathrm{Eff}} \cdot L \cdot s_0 \cdot b_0}}\right) \tag{A.25}$$

Surface mass on the sidewalls of the pleat

The surface mass density of the dust cake is defined as the deposited mass per unit filter area. Assuming a homogeneous cake layer with thickness τ and effective density ρ_{eff}, the local cake mass per unit area is given by τ.

Thus, the corresponding mass per unit area follows as:

$$W = \rho_{\mathrm{Eff}} \cdot \tau(\mathrm{t}) \tag{A.26}$$

Pressure drop

With Eq. (3) the resulting pressure drop for the sidewall model can be calculated with:

$$\Delta p = w_{\text{Filter}} \left(K_1' + K_2' \cdot W\right) \tag{A.27}$$

Appendix B. Differential pressure curves for comparable regeneration of different filter media geometries

The Appendix B offers further information concerning the comparability of the regeneration intensity of the different geometries. In this study the maximum peak pressure was used as reference and target variable for the regeneration intensity. The regeneration of cleanable filter media is influenced by more factors, such as the duration of the mechanical pressure pulse and the position inside the filter element.

Many studies investigating the pulse intensity in cartridge filters measure the intensity at different positions over the height of the cartridge. Feng et al. [52] placed three measuring points over 700 mm, Li et al. [35] measured the intensity every 230 mm over a filter length of 660 mm, and Ren et al. [34] measured the peak pressure at 100 mm, 500 mm, and 900 mm in a 1000 mm filter cartridge . Thus, the spacing between adjacent measurement locations in previous studies ranged from approximately 200–400 mm, which is considerably larger than the total height of the filter element investigated in the present study (90 mm). Due to the comparatively short filter element, whose total height is smaller than the spacing between measurement locations reported in previous studies the regeneration intensity was measured only at the center of the filter element (45 mm). The measuring point in the center was considered a reasonable approximation of the regeneration intensity over the entire element.

To supplement the evaluation based on the maximum peak pressure the duration of the mechanical pressure pulse for the different geometries was considered. The duration is defined by the time, in which the differential pressure signal is positive, indicating flow reversal by the pulse-jet. The pressure–time curves for the different geometries are shown in Fig. B.1. Each curve depicts the mean value of five intensity measurements and standard deviation is shown in light colors around the curves.

The differential pressure curves shown in Fig. B.1 show a similar overall trend. After a steep increase of differential pressure curves for PR2–PR5 decrease, only to rise again after about 180 ms. The secondary rise is due to the continuous filling of the pressure tank with pressurized air. The continuous filling enables more pressurized air to be released while the valve is open, resulting in the maximum peak pressure for PR2–PR5. The differences in maximum peak pressure are small and are attributed primarily to sample-to-sample variations in filter media

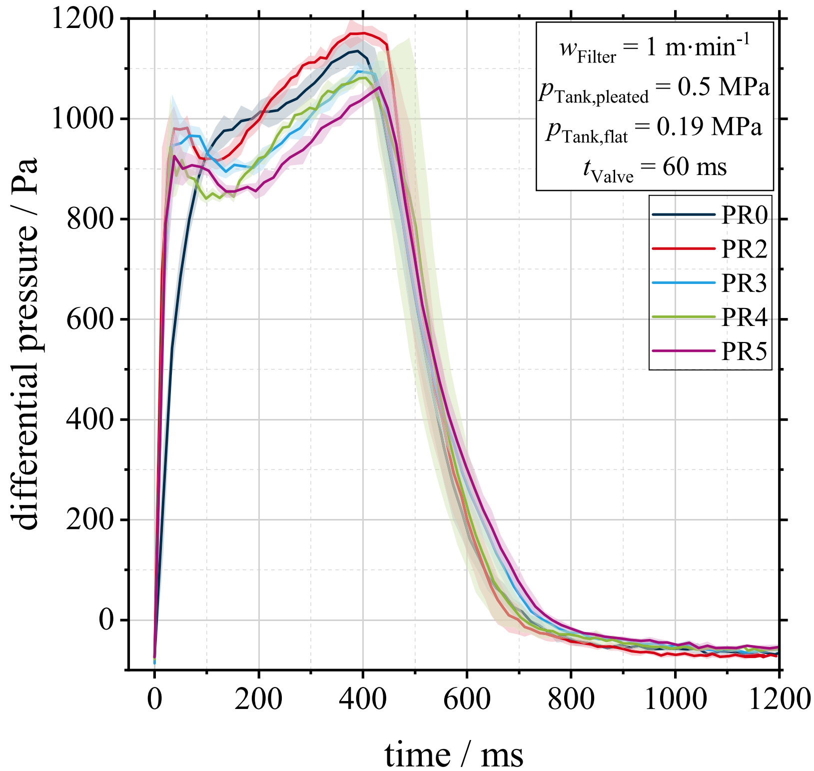

Fig. B.1. Mean differential pressure curves during regeneration for PR0 and PR2–PR5 for unused filter media.

resistance and can be neglected, as discussed in Section 2.1.4. The differential pressure curve for PR0 differs slightly, as the initial slope of the increase is smaller, compared to PR2–PR5 and no secondary peak can be observed. This is likely caused by the decreased tank pressure of 0.19 MPa. Nevertheless, the duration of the differential pressure pulse is similar for each geometry with a duration of 700–750 ms. Slight deviations in duration can occur due to the closing time of the valve, which can vary slightly or electrical latencies, which can influence the electrical opening time of the valve slightly.

Data availability

Data will be made available on request.

References

[1] F. Löffler, Staubabscheiden, in: Lehrbuchreihe Chemieingenieurwesen / Verfahrenstechnik, Georg Thieme, Stuttgart, 1988.

[2] E. Schmidt, Abscheidung von Partikeln aus Gasen mit Oberflächenfiltern, in: Fortschritt-Berichte VDI, Vol. 3, VDI Verlag GmbH, Düsseldorf, 1998.

[3] E. Bakke, Optimizing filtration parameters, J. Air Pollut. Control Assoc. 24 (12) (1974) 1150–1154, http://dx.doi.org/10.1080/00022470.1974.10470027.

[4] A. Dittler, M.V. Ferer, P. Mathur, P. Djuranovic, G. Kasper, D.H. Smith, Patchy cleaning of rigid gas filters—Transient regeneration phenomena comparison of modelling to experiment, Powder Technol. 124 (1–2) (2002) 55–66, http://dx.doi.org/10.1016/S0032-5910(01)00481-8.

[5] J. Binnig, J. Meyer, G. Kasper, Origin and mechanisms of dust emission from Pulse-Jet cleaned filter media, Powder Technol. 189 (1) (2009) 108–114, http://dx.doi.org/10.1016/j.powtec.2008.06.012.

[6] L.-M. Lo, D.-R. Chen, D.Y.H. Pui, Experimental study of pleated fabric cartridges in a Pulse-Jet cleaned dust collector, Powder Technol. 197 (3) (2010) 141–149, http://dx.doi.org/10.1016/j.powtec.2009.09.007.

[7] N. Grosjean, D. Iliev, O. Iliev, R. Kirsch, Z. Lakdawala, M. Lance, M. Michard, A. Mikelić, Experimental and numerical study of the interaction between fluid flow and filtering media on the macroscopic scale, Sep. Purif. Technol. 156 (2015) 22–27, http://dx.doi.org/10.1016/j.seppur.2015.09.010.

[8] R.J. Wakeman, N.S. Hanspal, A.N. Waghode, V. Nassehi, Analysis of pleat crowding and medium compression in pleated cartridge filters, Chem. Eng. Res. Des. 83 (10) (2005) 1246–1255, http://dx.doi.org/10.1205/cherd.04183.

[9] A.N. Waghode, N.S. Hanspal, R.J. Wakeman, V. Nassehi, Numerical analysis of medium compression and losses in filtration area in pleated membrane cartridge filters, Chem. Eng. Commun. 194 (8) (2007) 1053–1064, http://dx.doi.org/10.1080/00986440701293140.

[10] M. Rebaï, M. Prat, M. Meireles, P. Schmitz, R. Baclet, A semi-analytical model for gas flow in pleated filters, Chem. Eng. Sci. 65 (9) (2010) 2835–2846, http://dx.doi.org/10.1016/j.ces.2010.01.014.

[11] C.-W. Chen, S.-H. Huang, C.-M. Chiang, T.-C. Hsiao, C.-C. Chen, Filter quality of pleated filter cartridges, Ann. Occup. Hyg. 52 (3) (2008) 207–212, http://dx.doi.org/10.1093/annhyg/men008.

[12] L. Li, J. Yin, T. Sun, J. Chen, S. Fu, Y. Zhou, Z. Sun, Optimization design of pleated filter structure based on a simple theoretical model, Sep. Purif. Technol. 360 (2025) 131067, http://dx.doi.org/10.1016/j.seppur.2024.131067.

[13] F. Théron, A. Joubert, L. Le Coq, Numerical and experimental investigations of the influence of the pleat geometry on the pressure drop and velocity field of a pleated fibrous filter, Sep. Purif. Technol. 182 (2017) 69–77, http://dx.doi.org/10.1016/j.seppur.2017.02.034.

[14] P.-C. Gervais, S. Poussier, N. Bardin-Monnier, G. Karcher, D. Thomas, Combination of single-photon emission and X-Ray computed tomography to visualize aerosol deposition in pleated filter, Sep. Purif. Technol. 126 (2014) 52–61, http://dx.doi.org/10.1016/j.seppur.2014.02.011.

[15] S. Fotovati, S.A. Hosseini, H. Vahedi Tafreshi, B. Pourdeyhimi, Modeling instantaneous pressure drop of pleated thin filter media during dust loading, Chem. Eng. Sci. 66 (18) (2011) 4036–4046, http://dx.doi.org/10.1016/j.ces.2011.05.038.

[16] G. Teng, G. Shi, J. Zhu, Influence of pleated geometry on the pressure drop of filters during dust loading process: Experimental and modelling study, Sci. Rep. 12 (1) (2022) 20331, http://dx.doi.org/10.1038/s41598-022-24838-7.

[17] S. Li, A. Zhou, G. Peng, H. Jin, Q. Guo, J. Chai, C. Gui, Y. Luo, X. She, W. Liu, Simulation of pressure drop in pleated filter media during dust loading using an improved CFD porous media model, Powder Technol. 464 (2025) 121240, http://dx.doi.org/10.1016/j.powtec.2025.121240.

[18] Y. Alilou, S. Bourrous, T. Gélain, N. Bardin-Monnier, D. Thomas, Airflow characterization within the pleat channel of HEPA filters with mini pleats, Can. J. Chem. Eng. 99 (S1) (2021) http://dx.doi.org/10.1002/cjce.24025.

[19] Z. Feng, W. Pan, Y. Wang, Z. Long, Modeling filtration performance of pleated fibrous filters by Eulerian-Markov method, Powder Technol. 340 (2018) 502–510, http://dx.doi.org/10.1016/j.powtec.2018.09.037.

[20] M. Rebai, M. Prat, M. Meireles, P. Schmitz, R. Baclet, Clogging modeling in pleated filters for gas filtration, Chem. Eng. Res. Des. 88 (4) (2010) 476–486, http://dx.doi.org/10.1016/j.cherd.2009.08.014.

[21] K. Cheng, J. Zhu, F. Qian, B. Cao, J. Lu, Y. Han, CFD–DEM simulation of particle deposition characteristics of pleated air filter media based on porous media model, Particuology 72 (2023) 37–48, http://dx.doi.org/10.1016/j.partic.2022.02.003.

[22] A.M. Saleh, S. Fotovati, H. Vahedi Tafreshi, B. Pourdeyhimi, Modeling service life of pleated filters exposed to Poly-Dispersed aerosols, Powder Technol. 266 (2014) 79–89, http://dx.doi.org/10.1016/j.powtec.2014.06.011.

[23] A.M. Saleh, H. Vahedi Tafreshi, A simple Semi-Numerical model for designing pleated air filters under dust loading, Sep. Purif. Technol. 137 (2014) 94–108, http://dx.doi.org/10.1016/j.seppur.2014.09.029.

[24] J.-U. Kim, J. Hwang, H.-J. Choi, M.-H. Lee, Effective filtration area of a pleated filter bag in a Pulse-Jet bag house, Powder Technol. 311 (2017) 522–527, http://dx.doi.org/10.1016/j.powtec.2017.02.013.

[25] J.S. Kim, M.-H. Lee, Measurement of Effective Filtration Area of pleated bag filter for Pulse-Jet cleaning, Powder Technol. 343 (2019) 662–670, http://dx.doi.org/10.1016/j.powtec.2018.11.080.

[26] C. Guo, J. Kang, D. Wang, Y. Liang, L. Wang, G. Xu, H. Wang, M. Tang, Experimental and simulation study of particle deposition characteristics and pressure drop evolution in pleated filter media, Processes 13 (4) (2025) 975, http://dx.doi.org/10.3390/pr13040975.

[27] G. Teng, G. Shi, J. Zhu, J. Qi, C. Zhao, Research on the influence of pleat structure on Effective Filtration Area during dust loading, Powder Technol. 395 (2022) 207–217, http://dx.doi.org/10.1016/j.powtec.2021.09.062.

[28] Y. Cuiping, H. Wanlan, X. Feng, F. Junzhe, L. Yang, P. Yuyan, W. Yunduan, M. Ruizhi, The effect of pleat ratio on the Effective Filtration Area of the Large-Diameter pleated filter cartridge, Part. Sci. Technol. 42 (6) (2024) 1031–1042, http://dx.doi.org/10.1080/02726351.2024.2320099.

[29] G. Teng, C. Zhao, G. Li, W. Geng, Mechanism of interpleat channel blockage in pleated filters during dust loading, Sci. Rep. 16 (1) (2026) 19991, http://dx.doi.org/10.1038/s41598-026-51067-z.

[30] B.H. Park, M.-H. Lee, Y.M. Jo, S.B. Kim, Influence of pleat geometry on filter cleaning in PTFE/Glass composite filter, J. Air Waste Manage. Assoc. 62 (11) (2012) 1257–1263, http://dx.doi.org/10.1080/10962247.2012.696530.

[31] S. Li, S. Hu, B. Xie, H. Jin, J. Xin, F. Wang, F. Zhou, Influence of pleat geometry on the filtration and cleaning characteristics of filter media, Sep. Purif. Technol. 210 (2019) 38–47, http://dx.doi.org/10.1016/j.seppur.2018.05.002.

[32] J. Sievert, F. Löffler, Fabric cleaning in Pulse-Jet filters, Chem. Eng. Process.: Process. Intensif. 26 (2) (1989) 179–183, http://dx.doi.org/10.1016/0255-2701(89)90010-X.

[33] Q. Zhang, D. Liu, M. Wang, Y. Shu, H. Xu, H. Chen, Characteristics and evaluation index of Pulse-Jet dust cleaning of filter cartridge, Process. Saf. Environ. Prot. 157 (2022) 362–374, http://dx.doi.org/10.1016/j.psep.2021.11.028.

[34] L. Ren, N. Yuan, L. Lin, C. He, C. Tang, Z. Xu, Effect of jet airflow deflection on cleaning performance of filter Cartridge, Environ. Sci. Pollut. Res. 29 (18) (2022) 27510–27520, http://dx.doi.org/10.1007/s11356-021-18028-7.

[35] J. Li, S. Li, F. Zhou, Effect of cone installation in a pleated filter Cartridge during Pulse-Jet cleaning, Powder Technol. 284 (2015) 245–252, http://dx.doi.org/10.1016/j.powtec.2015.06.071.

[36] J. Qiu, D. Wu, D.-R. Chen, J. Li, Reverse Pulsed-Flow cleaning of pleated filter Cartridges having an inner pleated filter cone, Process. Saf. Environ. Prot. 146 (2021) 481–489, http://dx.doi.org/10.1016/j.psep.2020.11.025.

[37] C. Yan, G. Liu, H. Chen, Effect of induced airflow on the surface static pressure of pleated fabric filter Cartridges during pulse jet cleaning, Powder Technol. 249 (2013) 424–430, http://dx.doi.org/10.1016/j.powtec.2013.09.017.

[38] Q. Li, M. Zhang, Y. Qian, F. Geng, J. Song, H. Chen, The relationship between peak pressure and residual dust of a Pulse-Jet Cartridge Filter, Powder Technol. 283 (2015) 302–307, http://dx.doi.org/10.1016/j.powtec.2015.05.038.

[39] Q. Wu, X. Li, Z. Xing, Q. Kuang, J. Li, S. Huang, H. Huang, Z. Ma, D. Wu, Inhibition of dust re-deposition for filter cleaning using a multi-pulsing jet, Atmosphere 14 (7) (2023) 1173, http://dx.doi.org/10.3390/atmos14071173.

[40] K. Furumoto, T. Narita, T. Fukasawa, T. Ishigami, H.-P. Kuo, A.-N. Huang, K. Fukui, Influence of Pulse-Jet cleaning interval on performance of compact dust collector with pleated filter, Sep. Purif. Technol. 279 (2021) 119688, http://dx.doi.org/10.1016/j.seppur.2021.119688.

[41] Z. Xing, G. Wang, J. Guo, W. Lu, Y. Zhao, Q. Wu, J. Li, Improved pulsed-jet cleaning of cone filter cartridges using an annular-slit nozzle, Atmosphere 14 (9) (2023) 1332, http://dx.doi.org/10.3390/atmos14091332.

[42] B. Xie, H. Li, S. Hu, X. Zhang, Experimental study of an improved Pulse-Jet cleaning method to enhance performance of cartridge dust collectors, Powder Technol. 442 (2024) 119874, http://dx.doi.org/10.1016/j.powtec.2024.119874.

[43] D. Bémer, Y. Morele, R. Régnier, Filtration of ultrafine metallic particles in industry, Environ. Technol. 36 (18) (2015) 2374–2380, http://dx.doi.org/10.1080/09593330.2015.1028471.

[44] D. Bémer, R. Régnier, Y. Morele, F. Grippari, J.-C. Appert-collin, D. Thomas, Study of clogging and cleaning cycles of a pleated cartridge filter used in a thermal spraying process to filter ultrafine particles, Powder Technol. 234 (2013) 1–6, http://dx.doi.org/10.1016/j.powtec.2012.09.035.

[45] Z. Chen, B. Bao, W. Zhu, Z. Lin, Effect of test dust on performance test for a pleated filter cartridge, Aerosol Air Qual. Res. 15 (6) (2015) 2436–2444, http://dx.doi.org/10.4209/aaqr.2015.02.0125.

[46] Air Quality - Test Method for Filtration Characterization of Cleanable Filter Media (ISO 11057:2011), Internationale Norm DIN ISO 11057:2011, DIN, Berlin, 2012.

[47] J.P. Knisley, J. Meyer, A. Dittler, Methodology for the characterization of pleated filter media in a Pulse-Jet-Cleaned Test-Rig in accordance to DIN iso 11057, Sep. Purif. Technol. 389 (2026) 136720, http://dx.doi.org/10.1016/j.seppur.2025.136720.

[48] Filtering Separators - Surface Filtration, Beuth Verlag GmbH VDI 3677 Part 1, Verein Deutscher Ingenieure e.V., Düsseldorf, 2023.

[49] P. Bächler, J. Meyer, A. Dittler, Characterization of the emission behavior of Pulse-Jet cleaned filters using a low-cost particulate matter sensor, Gefahrstoffe 79 (11–12) (2019) 443–450.

[50] O. Kurtz, J. Meyer, G. Kasper, Influence of filter operating parameters on fine dust emissions from pulse-cleaned filter bags, Chem. Eng. Technol. 39 (3) (2016) 435–443, http://dx.doi.org/10.1002/ceat.201500340.

[51] J.E. Yit, B.T. Chew, Y.H. Yau, The study of pleat geometry on the air filtration performance, Indoor Built Environ. 32 (5) (2023) 902–913, http://dx.doi.org/10.1177/1420326X221145413.

[52] X. Feng, F. Geng, H. Teng, S. Li, J. An, C. Gui, Dust dispersion during the pulse-jet cleaning process with the diffuser effect of the Cartridge Filter, Environ. Sci. Pollut. Res. 30 (14) (2023) 41486–41504, http://dx.doi.org/10.1007/s11356-022-24865-x.